Low-invasive, wide-field, and cellular resolution two-photon imaging of neural population activity in brainstem and nucleus tractus solitarii

Authors:

Masakazu Agetsuma[1,2,3,*], Azumi Hatakeyama[3], Daisuke Yamada[3,*], Hiroshi Kuniishi[4], Eri Takeuchi[5], Shinji Tsuji[1], Chihiro Ito[2], Tomoko Kobayashi[1], Atsushi Noritake[6], Yoshitsugu Aoki[5], Hiroshi Yukawa[2], Akiyoshi Saitoh[3], Junichi Nabekura[1], Masayuki Sekiguchi[3,5]

Affiliations:

[1]Division of Homeostatic Development, National Institute for Physiological Sciences, 38 Nishigohnaka Myodaiji-cho, Okazaki, Aichi, 444-8585, Japan

[2] Quantum Regenerative and Biomedical Engineering Team, Institute for Quantum Life Science, National Institutes for Quantum Science and Technology (QST), Anagawa 4-9-1, Chiba Inage-ku, Chiba 263-8555, Japan

[3] Laboratory of Pharmacology, Faculty of Pharmaceutical Sciences, Tokyo University of Science, 2641 Yamazaki, Noda, Chiba 278-8510, Japan

[4]Division of Development of Mental Functions, Research Center for Child Mental Development, University of Fukui, 23-3, Matsuokashimoaizuki, Eiheiji-cho, Yoshida-gun, Fukui 910-1193, Japan

[5]Department of Molecular Therapy, National Institute of Neuroscience, National Center of Neurology and Psychiatry, 4-1-1 Ogawahigashi, Kodaira, Tokyo 187-8502, Japan.

[6]Division of Behavioral Development, Department of System Neuroscience, National Institute for Physiological Sciences, 38 Nishigohnaka Myodaiji-cho, Okazaki, Aichi, 444-8585, Japan

*Corresponding author. Email: age@nips.ac.jp, yamadada@rs.tus.ac.jp

Keywords:
Brain-viscera communication
Emotion
Two photon live brain imaging
Nucleus tractus solitarii
Vagus nerve stimulation
Brainstem

Summary: Brain-viscera communication plays a crucial role in regulating mental health, with the vagus nerve being a key structure mediating this interaction. Clinically, artificial vagus nerve stimulation (VNS) is used to treat various neuropsychiatric disorders, highlighting the importance of vagal afferent fibers in regulating emotion. The nucleus tractus solitarii (NTS) is a brainstem structure proposed to receive signals from vagal afferents and relay them to brain networks for emotion regulation. However, due to the anatomical complexity and difficulty in accessing the deep-brain NTS region in living animals, the mechanisms remain unclear. Here, we developed a wide-field and deep-brain two-photon imaging method using a double-prism based optical interface. This approach enables the identification of cellular-resolution neural activities in the NTS while preserving the cerebellum, which covers the NTS and is important for emotion regulation, intact. We systematically evaluated how NTS neurons respond to VNS and a gastrointestinal hormone, suggesting the usefulness of this method for investigating the role of the vagus-NTS pathway *in vivo*.

Introduction

Optical techniques are powerful for measuring and artificially manipulating neuronal activity to elucidate the function of neuronal circuits and dynamic information processing in the brain. These techniques have been widely used in rodent brain research. However, technical limitations remain in accessing deep brain regions. For example, the brainstem, a key deep-brain region for brain-viscera communication, has been difficult to optically investigate its physiological properties.

Regulating emotion through brain-viscera communication has received significant attention, and the abnormal communication is linked to neuropsychiatric disorders[1-6]. Afferent vagus fibers originating in the nodose ganglion in the cervical cord play a crucial role in brain-viscera communication, receiving information from various internal organs and relaying it to the central nervous system through the brainstem area[5,6]. Artificial vagus nerve stimulation (VNS), which is clinically applied to treat various neurological and psychiatric disorders[7-9], mainly target the afferent vagus nerve. Initially reported in the 19th century, the FDA approved VNS for treating drug-resistant seizures in 1997 and depression in 2005[10,11]. Currently, several neuropsychiatric and related disorders are considered potentially treatable with VNS[12]. For safe and effective VNS, the parameter

settings must be carefully optimized[13,14]. Research using rodent models is crucial for this optimization by elucidating the mechanisms underlying VNS and its therapeutic effects. Previous studies in rodents demonstrated that VNS effectively suppresses seizures[15,16], mitigates cerebral ischemia[17], and treats chronic pain[18]. Furthermore, VNS significantly reduces depressive symptoms[19,20] and facilitates the extinction of associative fear memory[21]. These findings suggest that the insights gained from animal models are critical to advancing VNS-based clinical treatments and understanding the mechanisms of emotion regulation through the vagus nerve.

Previous studies have indicated that the nucleus tractus solitarii (NTS) is likely a critical gateway for regulating emotions through brain-viscera communication and for VNS-based clinical treatments[6,8,22,23]. Afferent vagus fibers receive information from various internal organs and are proposed to relay it to the NTS[6,23-26]. The NTS projects to various brain regions involved in emotion regulation, such as the amygdala, lateral hypothalamic area, bed nucleus of the stria terminalis, and periaqueductal gray[6,8], which suggest the involvement of the vagus-NTS pathway in regulating emotion. VNS has also been shown to modulate the activity of various brain regions[27-29], including the locus coeruleus, whose activity is regulated by the NTS. Lesions of the locus coeruleus suppress the anti-epileptic effects of VNS[15]. The actual role of the NTS and the detailed mechanisms underlying the therapeutic effects of VNS, however, remain unclear. It is also unclear how information from various organs relayed to the NTS for regulating emotion is processed, and whether the information from various organs is segregated or integrated within the NTS.

Addressing these questions has been challenging because the NTS is located deep in the brain and is surrounded by regions critically involved in vital functions, making direct observation difficult. Removing the cerebellum to expose the brainstem allows for observations of a wide area of the brainstem including the NTS, which is useful to study the role of the NTS in regulating the information from the digestive systems[30]. However, the cerebellum is also an essential brain structure for emotional regulation[31-34] and is modulated by the VNS-based treatment[28]. Therefore, the development of a novel technique for *in vivo* recordings of brainstem neurons without removing the cerebellum is in high demand. A technique to optically access the brainstem and NTS in the deep brain area while keeping the cerebellum intact would expand the possibilities for neural

activity imaging and optogenetic neural activity manipulation, thereby profoundly advancing our understanding of the function of the NTS and its contribution to emotional regulation.

This aim motivated us to develop an *in vivo* two-photon imaging technique using a double-prism based optical interface (Double-Prism based brainStem imaging under Cerebellar Architecture and Neural circuits, "D-PSCAN"). The D-PSCAN method enables the observation of neural population activity with single-cell resolution in the brainstem and NTS situated deeply beneath the cerebellum while keeping the cerebellum and surrounding neural connections intact. We demonstrated the capability of this method to distinguish NTS activity from that of descending vagus neurons whose cell bodies lie ventrally to the NTS. The recorded neural activity data were used to evaluate the physiological characteristics of NTS neurons, i.e., their responsiveness to VNS. We also demonstrated the application of this imaging technique for detecting responsiveness to a gastrointestinal hormone cholecystokinin-8 (CCK), a more physiological stimulus than VNS. Our results suggest the applicability of this method for detailed understanding of the physiological mechanism of the NTS and future research on emotional regulation through the vagus-NTS pathway.

Results:

Double microprism for optical access to the brainstem area deep below the cerebellum

We developed a novel *in vivo* two-photon calcium imaging method for observing the deep brain area in mice that enables neural population activity recordings in the brainstem and NTS. Using a genetically encoded Ca^{2+} indicator, GCaMP, expressed by an adeno-associated virus (AAV), we aimed to detect neural activities in the NTS (Figure 1A–B) to observe the responsiveness of NTS neurons to various stimuli. Viruses encoding GCaMP were injected into the NTS at approximately postnatal day (P) 50–60 for *in vivo* imaging experiments, at least 1 month before the microprism implantation described below. Although primarily targeted at the NTS, viruses often spread to adjacent areas, beneficially inducing additional expression in surrounding regions and allowing us to visualize wide areas of the brainstem.

The brainstem is located deeply below (2.0–2.5 mm) the dorsal surface of the cerebellum. One potential problem in observing neural activities in the brainstem is that

134 even when the mouse head is fixed under the objective lens for two-photon imaging by
135 tightly attaching the head plate to the skull, the brainstem can still move somewhat
136 independently in response to the mouse's body movements[30]. Although standard skull
137 reference points (bregma and lambda) are typically referred to when targeting specific
138 brain areas, it is also crucial to visually capture the brain structure under observation in
139 each mouse. In a previous study, the cerebellum was removed to address these issues[30],
140 but the cerebellum is also involved in emotion control[31]; therefore, to accurately elucidate
141 the role of the vagus-NTS pathway in regulating emotion, it is essential to have a wide
142 field of view of the brainstem while keeping the cerebellum and neural connections intact.
143 To achieve this aim, we developed a technique to optically access the deep brainstem
144 area using a double prism (Figure 1C–E). We designed an implantable double microprism
145 assembly comprising a 2-mm right-angle glass microprism bonded to another 2-mm
146 right-angle glass microprism and a 4 mm × 4 mm or 3 mm × 4 mm cover glass window at
147 the surface-end position of the imaging window (Figure 1C). Dental cement was used to
148 fix this assembly at the correct position for NTS imaging. The cover glass enhanced
149 adhesion to the dental cement, thereby securing the position of the double microprism
150 assembly and preventing dental cement from obstructing its optical path. We implanted
151 the assembly (simply termed "double prism") between the cerebellum and the brainstem
152 using a custom-made vacuum-based manipulator (Figure 1D and Figure S1A–C). To
153 implant the double prism, the skull over the dorsal surface of the cerebellum was carefully
154 removed using a dental drill and fine forceps (Figure S1D–E). A micro-knife was used to
155 incise the thick dura mater between the posterior edge of the cerebellum and the spinal
156 cord. Removing the dura mater over the cerebellum not only allows for smooth insertion
157 of the prism but also adequately relieves the pressure that might occur when the prism is
158 inserted between the cerebellum and brainstem.
159 Next, the newly developed vacuum-based prism holder was used to insert and implant
160 the double prism between the cerebellum and brainstem (Figure 1D–E, Figure S1C, F–
161 G). Sufficient space and no neural fibers remained between the cerebellum and brainstem
162 around the NTS area, enabling smooth insertion of the prism without cutting neural fibers.
163 Using a stereotaxic frame and vacuum-based prism holder attached to an equipped
164 manipulator, the prism can be precisely operated during the implantation while being
165 maintained in a horizontal position. The vacuum-based prism holder has a hook on one

166 side (Figure 1D and Figure S1B–C), which exerts a pushing force when sliding the sharp
167 corner of the double prism between the cerebellum and brainstem from the caudal side to
168 the rostral side (Figure 1D–E). After slowly inserting the double prism to approximately
169 1.6 mm deep, we waited a few minutes to ensure that breathing and other physical
170 conditions were not disturbed (Figure 1E). The double prism was slid further down at 0.1-
171 mm increments until reaching a maximum depth of 2.0 mm. Any physical reactions such
172 as disrupted breathing occurring during the insertion led us to promptly retract the prism.
173 Setting a stereomicroscope at an angle such that the brainstem can be visualized through
174 the double prism allows for clear observation of the arrangement of blood vessels in the
175 brainstem and fourth ventricle while inserting the prism.

176 After the double prism was fully inserted, UV craft resin was used to fix the double
177 prism and coat the surface of the targeted nerve structures (Figure S1G), followed by tight
178 fixation with dental cement. A resin coating was applied with the double prism remaining
179 in the holder and maintaining sufficient contact with the brainstem target area (including
180 the NTS) to prevent the resin from getting between them. After the UV resin had cured,
181 the holder was carefully released, and the double prism was firmly fixed to the
182 surrounding areas, including the remaining skull bone rostral to the cerebellum, using
183 dental cement. For further head fixation for two-photon imaging under the microscope
184 objective, the head plate was attached to the skull with dental cement (Figure 1F).

185 The double prism allows for optical access to the brainstem located on the ventral side
186 of the cerebellum, which exceeds 2.0 mm in thickness. Using the wide field of view and
187 horizontal coordinates, the position of the fourth ventricle serves as a key reference for
188 locating the NTS. Two-photon imaging through the double prism enabled us to detect
189 neural activities in the NTS at single-cell resolution, visualized by GCaMP (Figure 1G).
190 We named this method "D-PSCAN" as explained above.

191 We confirmed the specificity of the method for detecting NTS neural activities. A
192 primary purpose for developing this imaging method was to investigate how information
193 from afferent vagus nerve inputs is processed in the NTS. On the other hand, the dorsal
194 motor nucleus of the vagus nerve (10N, also known as DMNV or DMV), where the cell
195 bodies of the vagal efferent fibers originate, is located just ventrally to the NTS[6],
196 suggesting the importance of confirming specificity in the NTS and distinguishing NTS
197 neurons from 10N neurons. Importantly, the two-photon imaging technique offers

198 superior spatial resolution at depth. Based on this advantage, we confirmed that the
199 obtained signals originated from the brainstem surface area, i.e., the NTS, rather than
200 deeper regions such as 10N. To further test the specificity, we prepared fixed brain slices
201 after the *in vivo* imaging experiments and checked the expression of GCaMP within the
202 NTS. We used ChAT, an immunohistochemical marker, to identify 10N neurons[35] and
203 distinguish NTS neurons histologically. Expression of GCaMP was not observed in
204 ChAT-positive cells within 10N (Figure 1B), indicating that NTS neuron activities can
205 be detected separately from efferent vagus neuron activities using this method. We also
206 checked for unanticipated retrograde labeling of the vagal afferent terminals onto the NTS.
207 Cell bodies of vagus neurons projecting to the NTS are located in the nodose ganglion[6,36].
208 In mice that showed GCaMP expression in the NTS neurons, we observed no GCaMP-
209 expressing cell bodies in the nodose ganglion, i.e., vagus sensory neurons (Figure S2).
210 These findings demonstrated that, when imaging neural activities around the NTS region
211 using this method, we can distinguish activities of NTS neurons from the signals of vagal
212 afferent nerve terminals. Thus, the D-PSCAN method enables us to specifically evaluate
213 the activities of the NTS neurons separately from the activities of vagal efferent neurons
214 and vagal afferent fiber terminals.
215
216 *In vivo* imaging of neural population activities at single-cell resolution in the brainstem
217 (NTS) of live mice
218 Using the D-PSCAN method, we performed *in vivo* two-photon imaging and recorded
219 the neural population activities of the NTS and surrounding brainstem areas. Spontaneous
220 activities and stimulus-evoked responses of the brainstem neurons were recorded by
221 imaging GCaMP fluorescence changes (ΔF/F0). Brain motion artifacts interfered with
222 imaging in awake mice but were minimized under anesthesia, enabling stable detection
223 of the neural activities at a single-cell resolution both inside and outside of the NTS area
224 (Figure 2 and Supplementary Movie 1, 2). Time-lapse imaging at various depths was
225 performed by adjusting the imaging focal plane using a piezo to move up and down in
226 depth (Figure 2A and Figure S3). Volumetric live imaging (2 mm x 2 mm horizontally,
227 or smaller for zooming, 200–480 μm dorsoventrally, at 0.4–1.0 Hz temporal resolution)
228 of neural activities in the wide brainstem area (including the NTS) of the head-fixed

229 mouse was performed through the implanted double prism. Importantly, this wide field
230 of view and piezo-based volumetric imaging allowed us to detect GCaMP fluorescence
231 and neural activities not only from inside but also from outside of the NTS areas and to
232 confirm the specificity of the stimulus-evoked responses in the NTS, as explained below.
233

234 Detection of single cell activities in the NTS as the direct efferent target of the vagus
235 nerve

236 To demonstrate the usefulness of the D-PSCAN for investigating the physiological
237 characteristics of the NTS neurons, we applied the method to observe the neural responses
238 to artificial electrical stimulation of the afferent vagus nerve under various conditions
239 (vagus nerve stimulation, or VNS). We tested whether NTS neurons respond to the stimuli
240 and further evaluated the diversity of their responsiveness. To perform VNS, the bipolar
241 platinum hook electrode that has been used in rodents[37] was employed (Figure 2B). After
242 isolating the vagus nerve from the carotid artery, a bipolar platinum hook electrode was
243 wrapped around the left vagus nerve and fixed in place without contacting other tissues
244 using the insulating silicone adhesive (Kwik-Sil)[38,39]. The electrode was positioned to
245 keep the positive and negative poles apart. This setup allows for stable activation of the
246 vagus nerve while preventing irritation to the surrounding tissue. To create an anodal
247 block for the efferent direction, the cathode and anode were located on the rostral and
248 caudal sides, respectively, of the vagus nerve. The mechanism of the anodal block is
249 proposed to selectively bias activation toward vagal afferent fibers[40-44]. We selectively
250 targeted the left vagus nerve, which is usually chosen for safety reasons, as stimulation
251 of the right vagus nerve has a greater impact on heart rate[45,46]. We conducted *in vivo* NTS
252 imaging experiments after closing the surgical wound.

253 We imaged the *in vivo* neural activity in the brainstem as VNS was repeatedly applied.
254 The VNS parameters were established based on previous studies, and various conditions
255 (i.e., various current intensities and stimulus frequencies) within the ranges reported in
256 prior rodent and human studies[13,42,43,47] were used to investigate the neural response
257 properties. Figure 2C presents an example in which the stimulation intensity was set to
258 1.0 mA and the stimulation frequency was 10 Hz. A pulse width of 100 microseconds
259 (μsec) was consistently selected across all experiments in the present study. At a stimulus

260 frequency of 10 Hz, stimulation (100-μsec current) occurred 10 times per second. The
261 term "trial" is defined as each 10-sec VNS duration, while the term "session" is defined
262 as a series of VNS trials at each condition (e.g., 1.0 mA at 10 Hz, 0.5 mA at 10 Hz, 1.0
263 mA at 5 Hz, etc.). In each session, the inter-trial interval was set at 50 sec. In the example
264 cases shown in Figure 2, 10-sec VNS was repeated multiple times within a session to
265 assess the neural responses to each VNS condition.

266 Taking advantage of the 2 mm x 2 mm large field of view provided by the double
267 prism, we conducted volumetric observations of a wide brainstem area, including the NTS,
268 and compared neural responses to VNS inside and outside of the NTS (Figure 2D). In an
269 example case (Figure 2D), we scanned a total of 16 z-planes at each time point. We
270 stacked every 4 consecutive plane from top to bottom to create an average image for each
271 time point with carefully correcting the motion artifact (see Methods for details). This
272 stacking was done with a two-plane overlap; for instance, the first stack included the 1st
273 to 4th z-planes, the second stack included the 3rd to 6th z-planes, and subsequent stacks
274 followed this pattern. As a result, we obtained 7 stacked planes in total in this experiment,
275 labeled Zp1 through Zp7, respectively. This procedure is advantageous to enhance the
276 signal to noise ratio in each movie, which is critical for further automatic detection of the
277 active neurons[48]. The motion-corrected movies were analyzed to automatically detect the
278 active neurons using a constrained nonnegative matrix factorization algorithm, as
279 described previously[48,49]. This detection method is advantageous in isolating the activity
280 of the individual neuron, even when other active neurons are nearby or overlapped within
281 the field of view[48] (see Methods for details). After automatic detection of the active
282 neurons, we checked the existence of overlapped detection of the regions of interest (ROIs,
283 i.e., active neurons) between adjacent Zps, and removed such overlaps by manual
284 inspection.

285 Temporal dynamics of neural activity were clearly observed within the field of view
286 at multiple depths (Figure 2D and Supplementary Movie 1). Here, we present the GCaMP
287 signals at Zp1, Zp2, and Zp4. Neurons exhibiting stimulus-evoked and/or spontaneous
288 neural activity were automatically identified, and representative neurons are shown in the
289 graph. In the case of neurons outside of the NTS, we observed no clear responses to VNS
290 and detected only spontaneous (stimulus-independent) activities (neurons #1 and #2 in

291 Figure 2D). On the other hand, we detected a large number of neurons responding to VNS
292 in the NTS area (neurons #3–#21).
293 Two-photon imaging utilizes a scanning-type observation system, enabling seamless
294 transition from wide-field to high-magnification imaging using a single objective lens.
295 Depending on the point spread function of the objective lens, this approach facilitates the
296 acquisition of images with enhanced spatial resolution compared with maximum wide-
297 field imaging. Using this mechanism, after confirming the position of the NTS in the wide
298 field of view, we narrowed down the imaging area to the NTS and observed the neural
299 activities at high magnification (Figure 2E and Supplementary Movie 2). We detected
300 individual neuron cell bodies more clearly through visual inspection at higher
301 magnifications compared with lower magnifications, confirming that most neurons
302 identified at lower magnification were indeed NTS neuron cell bodies, which exhibited
303 clear responses to VNS.
304 Note that there was variability in VNS responsiveness among neurons detected within
305 the NTS (Figure 2D and E), prompting us to further examine their characteristics more
306 thoroughly by varying the stimulus conditions.
307
308 Diverse neuronal responses to VNS in the NTS
309 *In vivo* brainstem imaging was performed during VNS administered at various
310 intensities and frequencies to explore how NTS neurons respond to different intensities
311 and frequencies. Additionally, we assessed the responsiveness of the NTS neurons to
312 repetitive stimulation across different intensities and frequencies.
313 First, we set the stimulus frequency at 10 Hz and varied the stimulus intensities
314 (Figure 3A–E and Figures S4A, S5). Most of the stimulus-responsive NTS neurons
315 exhibited enhanced responses to higher stimulus intensities. On the other hand, one
316 neuron detected outside of the NTS showed only a spontaneous activity change and no
317 clear response to VNS (neuron #2 in Figure 3 and Figures S4, S5). NTS neurons showed
318 minimal responses to VNS at 0.1 mA and 0.25 mA and there was no clear difference
319 between these intensities, while there was a substantial increase in the neural response at
320 0.5 mA. The difference between 0.5 mA and lower intensities suggests a possible
321 threshold between them for recorded NTS neurons. At 1.0 mA, the responses increased

322 further. We also calculated various parameters for evaluating the neural responses and
323 observed consistent tendencies (Figure 3E).
324 We next evaluated the effect of repetitive stimulation on the neural responses at
325 various stimulus intensities (Figure 3C–D and Figure S4A). At 0.1 mA and 0.25 mA, we
326 did not observe a change in the responses to repeated stimulation (50-sec intervals) at
327 each stimulus intensity. On the other hand, at higher intensities of 0.5 mA and 1.0 mA,
328 some neurons exhibited gradually enhanced responses during the session with repeated
329 stimulations.
330 Next, using the same recorded neurons, we set the stimulus intensity at 1.0 mA and
331 varied the stimulus frequencies (Figure 3F–H and Figure S4B). The neuronal responses
332 to VNS increased gradually as the stimulus frequency was increased from 1 Hz to 10 Hz,
333 similar to when the stimulus intensity was increased. Interestingly, increasing the
334 frequency to 15 Hz resulted in a reduction in the neural response compared with that at
335 10 Hz. We also investigated the effects of repetitive stimulation during each session at
336 various frequencies. At 1 Hz, 2.5 Hz, and 5 Hz, we did not observe clear changes in
337 response to repeated stimulation during each session. At 10 Hz, however, most of the
338 NTS neurons showed a gradually increased response. Notably, at a higher frequency of
339 15 Hz, despite similar initial responses to those at 10 Hz, neurons exhibited decreased
340 responses to subsequent stimuli during the session.
341 These results indicate that repeated stimulation may uniquely affect synaptic
342 interactions and signal transmission between the vagal afferent nerve and NTS neurons.
343 While we consider the physiological mechanisms behind the observed acceleration and
344 deceleration below in the discussion section, our findings also suggest that the frequency-
345 dependent increase and decrease in responses to VNS are not merely artifacts caused by
346 the slow off-kinetics of GCaMP. Changes in neural activities and associated calcium
347 concentrations occur more rapidly than the signal changes detected by calcium indicators
348 like GCaMP. This discrepancy can theoretically lead to an artificial amplification of
349 baseline signals during repetitive stimuli, which may account for the increase in
350 fluorescent signals at 10 Hz. Our imaging system, however, reliably detected an opposing
351 decrease in the GCaMP signal in response to repetitive stimulation at 15 Hz, despite
352 similar initial response levels to those observed at 10 Hz. Thus, the enhanced responses

353 at 10 Hz are also likely to reflect the actual responses of the neurons, rather than being
354 artifacts.
355 Together, these findings indicate that the D-PSCAN method effectively detects
356 various types of neurons in the NTS under different stimulus conditions. This method
357 demonstrated that specific VNS conditions can directly and effectively modulate NTS
358 neuron activities, potentially influencing whole-brain neural networks involved in the
359 regulation of emotion.
360
361 Chemical stimulation triggered both immediate and long-lasting responses in NTS
362 neurons
363 Up to this point, we examined the response of NTS neurons to artificial electrical
364 stimulation of the vagal afferent nerve. Emotional responses are also governed by more
365 physiological stimuli and conditions. To assess the suitability of the D-PSCAN method
366 for capturing responses under physiological conditions, we measured the activity of NTS
367 neurons following intravenous administration of CCK (Figure 4A). CCK is a hormone
368 released from the gastrointestinal tract after meals[50]. It directly influences the afferent
369 fibers of the vagus nerve[51] and is proposed to transmit signals via the NTS[51,52] to various
370 brain regions, including the feeding center.
371 To assess whether the intravenous administration process itself affects neural activity,
372 we also monitored responses during saline administration as a negative control. The
373 timing of the intravenous administration was determined by including SR101 in the
374 injected solution and observing the signal detected in the blood vessels surrounding the
375 NTS using *in vivo* two-photon microscopy (Supplementary Movie 3).
376 With this method, we first demonstrated that saline administration did not induce a
377 clear change in neural activity (Figure 4B–C and Supplementary Movie 4). In contrast,
378 CCK administration induced a change in NTS neuron activities (Figure 4B–C and
379 Supplementary Movie 5); upon administering CCK, we immediately observed clear and
380 significant signal changes in NTS neurons (Figure 4B–E). This immediate response of
381 the NTS neuron is consistent with a previous study demonstrating the responsiveness of
382 vagal afferents to CCK[53]. Additionally, for more than 5 minutes after CCK administration,
383 we observed a higher frequency of spontaneous activity compared with before CCK
384 administration or after saline administration (Figure 4C, F and Figure S6). This prolonged

activation in the NTS neuron is also consistent with the previous observation in vagal afferent fibers[53]. These results demonstrate that the D-PSCAN method is applicable to the detection of changes in NTS neuron activity induced under physiological conditions.

Discussion:

In the present study, to understand how the information processing mechanisms of brain-viscera pathways mediated by the NTS regulate emotions, we developed a new imaging technique named D-PSCAN based on *in vivo* two-photon imaging and double prism-based optical access. This method enables wide-field observation of deep-brain areas in the brainstem, including the NTS, while keeping the cerebellum, an important region for emotional regulation, intact. We confirmed that the D-PSCAN method allows for specific identification of NTS neurons, distinguishing them from surrounding regions based on horizontal coordinates in its wide field of view. Additionally, based on the advantages of two-photon imaging, we confirmed that the obtained signals originated from the surface brainstem area, i.e., the NTS, rather than deeper regions such as 10N. As we observed no GCaMP expression in 10N, it appears unlikely that vagal afferent terminals were labeled by GCaMP, ensuring almost no or undetectable contamination of their signal in the observed NTS areas. These findings together indicate that our method provides specific identification of NTS activities and assesses their responsiveness to VNS and CCK.

Using this method, we observed the responses of mouse NTS neurons to VNS, a technique clinically employed to treat neuropsychiatric disorders in humans. We confirmed that responses to electrical stimulation depended on the intensity and frequency, observed a threshold-like effect, and found that repeated excessive stimulation could reduce the responses. In addition to responses to artificial stimuli like VNS, we detected significant immediate responses and smaller but sustained activities following physiological stimuli such as CCK. These results demonstrate the usefulness of the D-PSCAN method for investigating how the NTS neurons process information from visceral organs for emotional regulation.

Recent studies have advanced our understanding of the complex mechanisms by which the NTS processes various types of visceral information[22,23,30,36,54]. How these mechanisms underlie the therapeutic effects of VNS and regulate emotion, however,

417 remains unclear. Our imaging technique, which allows for detailed observation of NTS
418 neuron activities while maintaining the integrity of cerebellar circuits crucial for
419 emotional regulation[31-34], is expected to be instrumental in deepening our knowledge of
420 these complex mechanisms.

421 Repeated VNS induced both enhanced and diminished NTS responses, depending on
422 the stimulus conditions. As discussed above, the observed NTS responses are unlikely to
423 be artifacts caused by the calcium indicator (GCaMP). These results indicate that repeated
424 stimulation may uniquely affect synaptic interactions and signal transmission between
425 the vagal afferent nerve and NTS neurons. Inhibitory interneurons in the NTS are
426 involved in information processing during mechanical stimulation of digestive organs[30,55],
427 suggesting the possible contribution of such complex circuitries within the NTS for
428 adjusting the VNS signal. The activity of NTS neurons during VNS might also be
429 modulated through interactions with other brain regions, including supramedullary
430 regions[56]. Therefore, our imaging method will be useful for future investigations into
431 these detailed regulatory mechanisms of the NTS. While an anodal block is likely to
432 enhance specificity in targeting vagal afferent fibers, VNS might also weakly stimulate
433 efferent fibers, which in turn might stimulate visceral organs and further activate the vagal
434 afferent fibers. This may also influence the rates of the neuron responses. Overall, as
435 optimizing VNS parameters for human patients is critical[13,14], our NTS imaging method
436 in mice could help reveal the underlying mechanisms of VNS, leading to more effective
437 and personalized therapy settings.

438 Previous electrophysiological studies suggest that CCK induces prolonged
439 activation of the vagal afferent nerve[53,57]. The CCK-evoked enhancement of the
440 spontaneous fluctuations in the GCaMP signal lasting for more than 5 minutes is
441 consistent with these electrophysiological observations. These results demonstrate that
442 the D-PSCAN method has significant potential to detect changes in NTS neuron activity
443 under physiological conditions.

444 Overall, our development of the wide-field and deep-brain two-photon imaging
445 method utilizing a prism-based optical interface marks a significant advancement in the
446 ability to study the NTS *in vivo* while maintaining an intact cerebellum. Future
447 applications of this imaging system, particularly in awake animals, will be crucial for
448 understanding the dynamic interactions within the NTS and its role in neuropsychiatric
449 disorders. By enabling detailed observation of NTS activities, this method offers a

powerful tool for advancing our understanding of the vagus nerve's impact on brain function and emotional health, potentially leading to improved clinical interventions for neuropsychiatric conditions.

Acknowledgements

We thank Okito Hashimoto for technical advice and discussion. We also thank the members of the laboratory for their help, especially Ikuko Takeda, Yuki Ichihashi, Ryo Fujikawa, and Fumiko Kito for experiments and data analyses. This study was supported by the JSPS KAKENHI Grant (grant number JP18K06536, JP20H05076, JP21H02801, JP22H05081, JP22H05519, JP24H01260 to M.A.), the Cooperative Study Program of National Institute for Physiological Sciences (19-233, 20-140 to M.S.; 21-244, 22NIPS218 to D.Y.), the practical research project for rare/intractable diseases from Agency for Medical Research and Development (AMED; Grant #: 20ek0109315h003 to M.S.), and the Research Grant for Neurological and Psychiatric Disorders from National Center of Neurology and Psychiatry, Japan (NCNP; Grant #: 30-3, 1-1, and 2-6 to M.S.).

Author Contributions

M.A., D.Y. and M.S. conceived and coordinated the whole project. M.A. designed and developed a method for double-prism-based *in vivo* two photon imaging with the support of T.K. and J.N.; M.A., D.Y., H.K., E.T. and M.S. performed imaging experiments during the VNS and CCK-administration; M.A., A.H., D.Y., and S.T. performed data analyses with the support of C.I., A.N., H.Y., A.S. and M.S.; M.A., A.H., D.Y., A.N., Y.A., and M.S. wrote the paper, with contributions from all authors.

Data availability

The data that support the findings of this study are available from the corresponding author upon reasonable request. The anatomical information in the Allen Brain Atlas (https://atlas.brain-map.org/) was used for the anatomical description, determination of the virus injection area, and evaluation of the recorded brain regions.

Methods

483 **Animals**. All animal experiments were carried out in accordance with National Institutes
484 of Health guidelines and approved by the National Institute for Physiological Sciences
485 Animal Care and Use Committee (approval number 18A102), or in accordance with the
486 National Institute of Neuroscience, National Center of Neurology and Psychiatry (Tokyo,
487 Japan) and were approved by the Institutional Animal Investigation Committee (approval
488 number: 2020004). Male C57BL/6 mice housed under a 12-h light/dark cycle with free
489 access to food and water were used for all experiments. Mice at 3–10 months of age were
490 used for the experiments.
491
492 **Virus injection**. Nucleus tractus solitarii (NTS) is a structure distributing in the dorsal
493 medulla near the area postrema. To express GCaMP, a genetically encoded calcium
494 indicator for monitoring neural activity, we used a gene expression system based on the
495 AAV vector. We tested AAV1/Syn.GCaMP6s, AAV1/Syn.GCaMP6f, and
496 AAVdj/Syn.GCaMP7f, which were produced as described previously[58,59] using plasmids
497 obtained from Addgene. As the GCaMP was expressed under the regulation of the Syn
498 (Synapsin) promoter, all of the recording targets were assumed to be neuron-specific. All
499 of the viruses allowed us to visualize the neural activity in the NTS, and type of virus
500 used in each experiment is indicated in each corresponding figure legend. Viruses were
501 injected into mice at approximately postnatal day (P) 50–60 for experiments at least 1
502 month before the microprism implantation, which was followed by *in vivo* imaging.
503 Injection procedures were performed as described previously[60], with some modifications
504 to target the NTS efficiently. During surgery, the mice were anesthetized with isoflurane
505 (initially 2% [partial pressure in air] and then reduced to 1%). A small circle (~1 mm in
506 diameter) of the skull was thinned over the cerebellum (around the injection site) using a
507 dental drill to mark the site for a small craniotomy. Viruses were injected into the bilateral
508 NTS regions at two sites (depth 4.7 and 3.7 mm from the dorsal surface of the cerebellum,
509 volume 250 nl/site, at 100 nl/min) to sufficiently cover the NTS, over a 5-min period at
510 each depth using a UMP3 microsyringe pump (World Precision Instruments). The X-Y
511 coordinates for the injection site were usually 0.5 mm lateral to the midline and 3.3 mm
512 caudal to lambda. The beveled side of the injection needle was faced to the caudal so that
513 the needle could be smoothly inserted into and passed through the cerebellum, and the
514 AAV would cover the NTS similarly in both hemispheres. We designed our injection
515 protocol (especially the volume and depth) carefully to widely cover the area around the

516 NTS, while the anatomical coordinates of the field of view for the two-photon imaging
517 were precisely targeted using visual guide through the microprism implanted as described
518 below (see the section "*In vivo* two-photon imaging in the wide brainstem area"). Also,
519 as shown in Figure 1B, the expression of GCaMP was excluded in the 10N area, which
520 placed next to and ventrally to the NTS as marked by the ChAT immunostaining. The
521 reason for the exclusion is unclear, but it may be because the promoters and/or serotypes
522 used in the present studies do not match for inducing the GCaMP expression in these
523 ChAT-positive neurons. In any case, since neurons in the 10N area receive synaptic inputs
524 from NTS neurons[6,61] and are a source of vagal efferents, the lack of expression in the
525 neurons of this area rather positively aids in the interpretation of the GCaMP signals
526 detected by *in vivo* NTS imaging. In some mice, a deeper area (more than 0.5 mm from
527 the dorsal surface of the brainstem, i.e., the surface of the microprism) also expressed the
528 GCaMP when the fluorescence was checked in the brain slices (Figure 1B), but this
529 deeper area was beyond the deepest limit of our two-photon imaging system for the
530 detection of the sufficient signal intensity through the double prism *in vivo*. These results
531 indicates that our recording system simply allows specific targeting of the neurons within
532 the NTS and together with laterally-surrounding wide areas.
533
534 ***In vivo* two-photon imaging in the wide brainstem area**. We developed a novel,
535 minimally invasive method based on the double prism, which allows *in vivo* two-photon
536 imaging of deep brain regions, specifically around the NTS. This innovative approach
537 also enables simultaneous vagus nerve stimulation (VNS) or intravenous administration
538 of cholecystokinin-8 (CCK).
539 *In vivo* two-photon imaging was performed as described previously[49,60], with some
540 special development for the optical access to the brainstem and NTS as explained below.
541 Before the surgery, we designed an implantable double microprism assembly, comprising
542 a 2-mm right-angle glass microprism (TS N-BK7, 2 mm AL+MgF2, Edmund) bonded to
543 another 2-mm right-angle glass microprism and a 3 mm x 3 mm, 3 mm × 4 mm or
544 4 mm × 4 mm cover glass window (No.1; Matsunami) at the surface-end position of the
545 imaging window, was prepared. Dental cement was used to fix this assembly at the correct
546 position for NTS imaging. The cover glass was used to enhance adhesion to the dental
547 cement, securing the position of the double microprism assembly and preventing dental
548 cement from obstructing its optical path. We implanted the assembly (or simply termed

549 "double prism") between the cerebellum and the brainstem using a custom-made vacuum-
550 based manipulator (Figure 1D and Figures S1A–C).
551 At 1–8 months after the virus injection, the mice were anesthetized with isoflurane
552 (initially 2% [partial pressure in air] and reduced to 1% during the surgery). For the
553 implantation of the double prism, the skull over the dorsal surface of the cerebellum was
554 carefully removed using a dental drill and fine forceps (Figure S1D–E). A micro-knife
555 was used to incise the thick dura mater between the posterior edge of the cerebellum and
556 the spinal cord. Removing the dura mater over the cerebellum not only allows for smooth
557 insertion of the prism but also adequately relieves the pressure that might occur when the
558 prism is inserted between the cerebellum and the brainstem.
559 Next, the newly developed vacuum-based prism holder was used to insert and implant
560 the double prism between the cerebellum and the brainstem (Figure 1D–E, Figure S1B–
561 C, F). Sufficient space and no neural fibers remained between the cerebellum and the
562 brainstem around the NTS area, enabling smooth insertion of the prism without cutting
563 neural fibers. Using a stereotaxic frame and vacuum-based prism holder attached to an
564 equipped manipulator, the prism can be precisely operated during the implantation while
565 being maintained in a horizontal position. The vacuum-based prism holder has a hook on
566 one side (Figure 1D and Figure S1B–C), which exerts a pushing force when sliding the
567 sharp corner of the double prism between the cerebellum and the brainstem from the
568 caudal side to the rostral side (Figure 1D–E). After slowly inserting the double prism to
569 approximately 1.6 mm deep, we waited a few minutes to ensure that breathing and other
570 physical conditions were not disturbed (Figure 1E). The double prism was slid further
571 down at 0.1-mm increments until reaching a maximum depth of 2.0 mm. Any physical
572 reactions such as disrupted breathing occurring during the insertion led us to promptly
573 retract the prism. When retracting the double prism assembly, it is crucial to ensure that
574 the suction force by the vacuum is sufficient, as insufficient suction may lead to failure
575 of the retraction. The area directly beneath the microprism was minimally compressed
576 but remained intact, minimizing motion artifacts caused by the animal's breathing. Setting
577 a stereomicroscope at an angle such that the brainstem can be visualized through the
578 double prism allows for clear observation of the arrangement of blood vessels in the
579 brainstem and fourth ventricle while inserting the prism. Bleeding was rarely observed
580 during the implantation procedure.

After the double prism was fully inserted, UV craft resin was used to fix the double prism and coat the surface of the targeted nerve structures (Figure S1G), followed by tight fixation with dental cement. A resin coating was applied with the double prism remaining in the holder and maintaining sufficient contact with the brainstem target area (including the NTS) to prevent the resin from getting between them. After the UV resin had cured, the holder was carefully released, and the double prism was firmly fixed to the surrounding areas, including the remaining skull bone rostral to the cerebellum, using dental cement. For the further head fixation for two-photon imaging under the microscope objective, the head plate was attached to the skull with dental cement (Figure 1F).

The double prism allows for optical access to the brainstem located on the ventral side of the cerebellum, which exceeds 2.0 mm in thickness. Using the wide field of view and horizontal coordinates, the position of the fourth ventricle serves as a key reference for locating the NTS. Two-photon imaging through the double prism enabled us to detect neural activities in the NTS at the single-cell resolution, visualized by GCaMP (Figure 1G). We named this method "D-PSCAN", or Double-Prism based brainStem imaging under Cerebellar Architecture and Neural circuits.

During the consecutive imaging sessions, mice were anesthetized with isoflurane (1%) or a ketamine (70 mg/kg) and xylazine (10.5 mg/kg) mixture (see the sections below for more details). Experiments were performed in a completely dark environment. The activity of NTS neurons was recorded by imaging fluorescence changes with a multiphoton microscope (Nikon A1R MP, Nikon) and a Mai Tai DeepSee Ti:sapphire laser (Spectra-Physics) at 920 nm, through a 4x dry objective, 0.28 N.A. (Olympus). Scanning and image acquisition were controlled by NIS-elements software (Nikon). Brain motion artifacts interfered with imaging in awake mice but were minimized under anesthesia, enabling the stable detection of the neural activities at a single cellular resolution both in and out of the NTS area (Figure 2, Figure S3 and Supplementary Movie 1 and 2). Time-lapse imaging at various depths was performed by adjusting the imaging focal plane using a piezo to move up and down in depth (Figure 2A and Figure S3). Volumetric live imaging (2 mm x 2 mm horizontally, or smaller for zooming, 200–480 μm dorsoventrally, at around 0.4–1.0 Hz temporal resolution) of neural activities in the wide brainstem area (including the NTS) of the head-fixed mouse was performed through the implanted double prism. Importantly, this wide field of view and piezo-based

volumetric imaging allowed us to detect the GCaMP fluorescence and neural activities not only from inside but also from outside of the NTS areas and confirm the specificity of the stimulus-evoked responses in the NTS, as explained below.

Vagus nerve stimulation during NTS imaging. For the NTS imaging experiments with vagus nerve stimulation (VNS), a bipolar platinum hook electrode, connected to a programmable stimulator (SEN-8203, NIHON KODEN, Tokyo, Japan) and isolator (SS-202J, NIHON KODEN), was wrapped around the cervical vagal trunk, and was fixed and insulated from surrounding tissue using the quick-setting silicone adhesive Kwik-Sil (World Precision Instruments, FL, USA). After separating the vagus nerve from the carotid artery, a bipolar platinum hook electrode was wrapped around the left vagus nerve and fixed in place without contacting other tissues using the insulating silicone adhesive, Kwik-Sil[38,39]. The electrode was positioned to keep the positive and negative poles apart. This setup allows for stable activation of the vagus nerve while preventing irritation to the surrounding tissue. To create an anodal block for the efferent direction, the cathode and anode were located on the rostral and caudal sides, respectively, of the vagus nerve. The mechanism of the anodal block is proposed to selectively bias activation toward vagal afferent fibers[40-44]. We selectively targeted the left vagus nerve, which is usually chosen for safety reasons, as stimulation of the right vagus nerve has a greater impact on heart rate[45]. We conducted *in vivo* NTS imaging experiments after closing the surgical wound.

The mouse's head was fixed under the objective lens by using the head plate tightly attached to the skull under anesthesia (a ketamine [70 mg/kg] and xylazine [10.5 mg/kg] mixture). VNS was triggered using custom Labview software. To determine optimal stimulation parameters VNS was delivered in blocked trials for 10 s at the frequencies of 1.0, 2.5, 5.0, 10, or 15 Hz, at the intensities of 0.1, 0.25, 0.5, or 1.0 mA, with a pulse width of 100 μsec. The maximum current intensity and frequency of stimulation were set at 1.0 mA and 10 Hz according to the previous study[37,47]. The first VNS train was delivered at least 10 s after the start of imaging, and VNS was repeated three times in total (Figure 3 and Figures S4, S5), or more (Figure 2), with a 50-sec interval. Neither facial nor muscle twitching (an indication of off-target stimulation of musculature surrounding the vagus nerve) was observed with any parameters used in any of the mice included in the present study. VNS and NTS imaging were performed with the mouse head fixed under the

645 microscope objective lens using the head plate. The timings of the imaging and VNS were
646 synchronously recorded with image acquisition (GCaMP imaging in NTS) using NI
647 software (Labview; National Instruments) and NI-DAQ (National Instruments).
648
649 **Intravenous administration of CCK during NTS imaging.** To examine the neural
650 activity change in response to more physiological stimulation than VNS, we employed
651 cholecystokinin octapeptide (CCK); it has been demonstrated that intravenous
652 administration of CCK activates vagal afferents and increases firing rate of hepatic branch
653 of the vagus nerve[53] (Cox and Randich, 1997). On the day of the experiment, mouse's
654 head was fixed under the objective lens by using the head plate tightly attached to the
655 skull under anesthesia (1% isoflurane). During the Ca^{2+} imaging, CCK solution (2.0
656 μg/kg) or saline was mixed with sulforhodamine 101 (SR101; 0.1 mM) and intravenously
657 administered through the tail vein. 60 sec after the start of the imaging, saline with SR101
658 was intravenously administered and performed for 10 minutes. Using the same animal,
659 60 sec after the beginning of the imaging, CCK with SR101 was intravenously
660 administered and performed for 15 minutes. Intravenous administration and NTS imaging
661 were performed with the mouse head fixed under the microscope objective lens using the
662 head plate.
663
664 **Imaging data analyses and statistics.**
665 The activity of NTS neurons was recorded by imaging fluorescence changes with a
666 multiphoton microscope (Nikon A1R MP, Nikon). Time-lapse imaging at various depths
667 was performed by adjusting the imaging focal plane using a piezo to move up and down
668 in depth (Figure 2A and Figure S3). The volumetric live imaging (at around 0.4–1.0 Hz
669 temporal resolution) of NTS neural activities was performed through the implanted
670 double prism. We recorded a total of 10–16 focal planes (z-planes) at each time point for
671 each mouse. In an example case (Figure 2D), we recorded a total of 16 z-planes at each
672 time point. We stacked every 4 consecutive plane from top to bottom to create an average
673 image for each time point. This stacking was done with a two-plane overlap; for instance,
674 the first stack included the 1st to 4th z-planes, the second stack included the 3rd to 6th z-
675 planes, and subsequent stacks followed this pattern. As a result, we obtained 7 stacked
676 planes in total in this experiment, labeled as Zp1 through Zp7, respectively. This
677 procedure is advantageous to enhance the signal to noise ratio in each movie, which is

critical for further automatic detection of the active neurons[48]. After the automatic detection of the active neurons (details for this detection method are described below), we checked the existence of the overlapped detection of the regions of interest (ROIs, i.e., active neurons) between adjacent Zps next each other, and removed such overlaps by the manual inspection.

Importantly, before stacking 4 consecutive z-planes at each time point as explained above, they were processed to correct for brain motion artifacts using the enhanced correlation coefficient image alignment algorithm[62]. For this z-axis correction, first (most dorsal surface frame) was used as a reference for correcting the second z-plane. Then, an average image of these two aligned z-planes was further used for the correction of the third z-plane. Eventually an average image of these three aligned z-planes was used for the motion correction of the fourth z-plane. Through this procedure, four z-planes were motion corrected and used to accurately obtain a stacked (averaged) image for each Zp at each time point. Next, the time-series of stacked GCaMP images at each Zp was further processed to correct for brain motion artifacts using the enhanced correlation coefficient image alignment algorithm[62]. Temporal dynamics of neural activity were clearly observed at multiple depths after this motion correction procedure (Supplementary Movies 1 and 2).

These motion-corrected movies were used for automatic ROI detection. The ROIs for the detection of neural activity were automatically selected using a constrained nonnegative matrix factorization algorithm in MATLAB R2014a/R2019b as described previously[48,49], with some manual adjustments as described above. This detection method is advantageous in isolating the activity of the individual neuron, even when other active neurons are nearby or overlapped in the field of view[48]. The same constrained nonnegative matrix factorization package for ROI detection also provides an option for signal processing and measurement of the signal change ($\Delta F/F$) of each neuron. We used this method to identify neurons and calculate $\Delta F/F$ for them. While neurons for the analyses were initially automatically detected, neurons responding to noisy signals with no apparent calcium transient at any time during the experimental days were identified by visual inspection and excluded from further analysis. To apply the same regions of interest (ROIs) for analyzing images obtained across multiple conditions (i.e., various VNS conditions or saline vs CCK experiments), the movies from the same mouse and the same field of view were precisely aligned with each other using the same enhanced

correlation coefficient algorithm as above, and these multiple movies of the same field of view were tentatively concatenated for the ΔF/F measurement. The obtained ΔF/F data were eventually separated to evaluate the neural responses under each condition.

For the statistical analysis, we used MATLAB R2022a/R2023b. The Wilcoxon signed-rank test for a paired comparison and the Kolmogorov-Smirnov test for a two-group comparison with pooled data (from all neurons) were used to determine statistical significance ($p < 0.05$) in Figure 4. Two-tailed tests were selected for all statistical analyses. Graphs were produced by MATLAB R2022a/R2023b.

As for the imaging data analysis, one concern was that the off kinetics of the GcaMP6f signal might not be sufficiently fast to consider the responses to 3 trails of VNS as independent data, and thus statistical evaluation based on these responses might not be reliable to evaluate the neural responses. As shown in Fig. 3G, however, neurons showed a reduced response to repeated stimulation, indicating that calcium signaling was not enhanced by delayed off-kinetics.

After the CCK administration, we observed prolonged neural activation, which was detected as continuous calcium transients (Figure 4 and Figure S6). To evaluate the event frequency of the transients, we identified the timing of the calcium transients by analyzing the first derivative of ΔF/F (Figure S6). The first derivatives of each neuron, from the entire imaging session (including both the saline and CCK experiments), were thresholded at 0.5 times the standard deviation to detect active time points. The onset of each event was then used to determine the timing of each transient. The intervals between calcium transient events were then calculated and used to compare the event frequencies between the saline and CCK experiments (Figure 4F).

Drugs

CCK was purchased from PEPTIDE INSTITUTE, INC. and was dissolved in saline (2.0 μg/kg). In addition, sulforhodamine (SR101), a red fluorescent dye, is diluted to 0.1 mM in saline or CCK solution to confirm the successful intravenous administration and the injection timing during NTS imaging.

References

1. Khalsa, S.S., Adolphs, R., Cameron, O.G., Critchley, H.D., Davenport, P.W., Feinstein, J.S., Feusner, J.D., Garfinkel, S.N., Lane, R.D., Mehling, W.E., et al. (2018). Interoception and Mental Health: A Roadmap. Biol Psychiatry Cogn Neurosci Neuroimaging *3*, 501-513. 10.1016/j.bpsc.2017.12.004.
2. Chen, W.G., Schloesser, D., Arensdorf, A.M., Simmons, J.M., Cui, C., Valentino, R., Gnadt, J.W., Nielsen, L., Hillaire-Clarke, C.S., Spruance, V., et al. (2021). The Emerging Science of Interoception: Sensing, Integrating, Interpreting, and Regulating Signals within the Self. Trends Neurosci *44*, 3-16. 10.1016/j.tins.2020.10.007.
3. Dantzer, R., O'Connor, J.C., Freund, G.G., Johnson, R.W., and Kelley, K.W. (2008). From inflammation to sickness and depression: when the immune system subjugates the brain. Nat Rev Neurosci *9*, 46-56. 10.1038/nrn2297.
4. Yamada, T., and Katagiri, H. (2007). Avenues of communication between the brain and tissues/organs involved in energy homeostasis. Endocr J *54*, 497-505. 10.1507/endocrj.kr-106.
5. D'Mello, C., and Swain, M.G. (2011). Liver-brain inflammation axis. Am J Physiol Gastrointest Liver Physiol *301*, G749-761. 10.1152/ajpgi.00184.2011.
6. Berthoud, H.R., and Neuhuber, W.L. (2000). Functional and chemical anatomy of the afferent vagal system. Auton Neurosci *85*, 1-17. 10.1016/S1566-0702(00)00215-0.
7. Beekwilder, J.P., and Beems, T. (2010). Overview of the clinical applications of vagus nerve stimulation. J Clin Neurophysiol *27*, 130-138. 10.1097/WNP.0b013e3181d64d8a.
8. Bonaz, B., Picq, C., Sinniger, V., Mayol, J.F., and Clarencon, D. (2013). Vagus nerve stimulation: from epilepsy to the cholinergic anti-inflammatory pathway. Neurogastroenterol Motil *25*, 208-221. 10.1111/nmo.12076.
9. Reid, S.A. (1990). Surgical technique for implantation of the neurocybernetic prosthesis. Epilepsia *31 Suppl 2*, S38-39. 10.1111/j.1528-1157.1990.tb05847.x.
10. Penry, J.K., and Dean, J.C. (1990). Prevention of intractable partial seizures by intermittent vagal stimulation in humans: preliminary results. Epilepsia *31 Suppl 2*, S40-43. 10.1111/j.1528-1157.1990.tb05848.x.

11. Groves, D.A., and Brown, V.J. (2005). Vagal nerve stimulation: a review of its applications and potential mechanisms that mediate its clinical effects. Neurosci Biobehav Rev *29*, 493-500. 10.1016/j.neubiorev.2005.01.004.
12. Wang, Y., Zhan, G., Cai, Z., Jiao, B., Zhao, Y., Li, S., and Luo, A. (2021). Vagus nerve stimulation in brain diseases: Therapeutic applications and biological mechanisms. Neurosci Biobehav Rev *127*, 37-53. 10.1016/j.neubiorev.2021.04.018.
13. Thompson, S.L., O'Leary, G.H., Austelle, C.W., Gruber, E., Kahn, A.T., Manett, A.J., Short, B., and Badran, B.W. (2021). A Review of Parameter Settings for Invasive and Non-invasive Vagus Nerve Stimulation (VNS) Applied in Neurological and Psychiatric Disorders. Front Neurosci *15*, 709436. 10.3389/fnins.2021.709436.
14. Heck, C., Helmers, S.L., and DeGiorgio, C.M. (2002). Vagus nerve stimulation therapy, epilepsy, and device parameters: scientific basis and recommendations for use. Neurology *59*, S31-37. 10.1212/wnl.59.6_suppl_4.s31.
15. Krahl, S.E., Clark, K.B., Smith, D.C., and Browning, R.A. (1998). Locus coeruleus lesions suppress the seizure-attenuating effects of vagus nerve stimulation. Epilepsia *39*, 709-714. 10.1111/j.1528-1157.1998.tb01155.x.
16. Krahl, S.E., Senanayake, S.S., and Handforth, A. (2001). Destruction of peripheral C-fibers does not alter subsequent vagus nerve stimulation-induced seizure suppression in rats. Epilepsia *42*, 586-589. 10.1046/j.1528-1157.2001.09700.x.
17. Jiang, Y., Li, L., Liu, B., Zhang, Y., Chen, Q., and Li, C. (2014). Vagus nerve stimulation attenuates cerebral ischemia and reperfusion injury via endogenous cholinergic pathway in rat. PLoS One *9*, e102342. 10.1371/journal.pone.0102342.
18. Shao, P., Li, H., Jiang, J., Guan, Y., Chen, X., and Wang, Y. (2023). Role of Vagus Nerve Stimulation in the Treatment of Chronic Pain. Neuroimmunomodulation *30*, 167-183. 10.1159/000531626.
19. Furmaga, H., Shah, A., and Frazer, A. (2011). Serotonergic and noradrenergic pathways are required for the anxiolytic-like and antidepressant-like behavioral effects of repeated vagal nerve stimulation in rats. Biol Psychiatry *70*, 937-945. 10.1016/j.biopsych.2011.07.020.

20. Krahl, S.E., Senanayake, S.S., Pekary, A.E., and Sattin, A. (2004). Vagus nerve stimulation (VNS) is effective in a rat model of antidepressant action. J Psychiatr Res *38*, 237-240. 10.1016/j.jpsychires.2003.11.005.
21. Noble, L.J., Souza, R.R., and McIntyre, C.K. (2019). Vagus nerve stimulation as a tool for enhancing extinction in exposure-based therapies. Psychopharmacology (Berl) *236*, 355-367. 10.1007/s00213-018-4994-5.
22. Andresen, M.C., and Kunze, D.L. (1994). Nucleus tractus solitarius--gateway to neural circulatory control. Annu Rev Physiol *56*, 93-116. 10.1146/annurev.ph.56.030194.000521.
23. Paton, J.F. (1999). The Sharpey-Schafer prize lecture: nucleus tractus solitarii: integrating structures. Exp Physiol *84*, 815-833.
24. Appleyard, S.M., Marks, D., Kobayashi, K., Okano, H., Low, M.J., and Andresen, M.C. (2007). Visceral afferents directly activate catecholamine neurons in the solitary tract nucleus. J Neurosci *27*, 13292-13302. 10.1523/JNEUROSCI.3502-07.2007.
25. Doyle, M.W., and Andresen, M.C. (2001). Reliability of monosynaptic sensory transmission in brain stem neurons in vitro. J Neurophysiol *85*, 2213-2223. 10.1152/jn.2001.85.5.2213.
26. Traub, R.J., Sengupta, J.N., and Gebhart, G.F. (1996). Differential c-fos expression in the nucleus of the solitary tract and spinal cord following noxious gastric distention in the rat. Neuroscience *74*, 873-884. 10.1016/0306-4522(96)00173-x.
27. Naritoku, D.K., Terry, W.J., and Helfert, R.H. (1995). Regional induction of fos immunoreactivity in the brain by anticonvulsant stimulation of the vagus nerve. Epilepsy Res *22*, 53-62. 10.1016/0920-1211(95)00035-9.
28. Chae, J.H., Nahas, Z., Lomarev, M., Denslow, S., Lorberbaum, J.P., Bohning, D.E., and George, M.S. (2003). A review of functional neuroimaging studies of vagus nerve stimulation (VNS). J Psychiatr Res *37*, 443-455. 10.1016/s0022-3956(03)00074-8.
29. Lomarev, M., Denslow, S., Nahas, Z., Chae, J.H., George, M.S., and Bohning, D.E. (2002). Vagus nerve stimulation (VNS) synchronized BOLD fMRI suggests that VNS in depressed adults has frequency/dose dependent effects. J Psychiatr Res *36*, 219-227. 10.1016/s0022-3956(02)00013-4.

30. Ran, C., Boettcher, J.C., Kaye, J.A., Gallori, C.E., and Liberles, S.D. (2022). A brainstem map for visceral sensations. Nature *609*, 320-326. 10.1038/s41586-022-05139-5.
31. Adamaszek, M., Manto, M., and Schutter, D.J.L.G. (2022). The Emotional Cerebellum https://doi.org/10.1007/978-3-030-99550-8.
32. Supple, W.F., Jr., and Leaton, R.N. (1990). Cerebellar vermis: essential for classically conditioned bradycardia in the rat. Brain Res *509*, 17-23. 10.1016/0006-8993(90)90303-s.
33. Supple, W.F., Jr., and Kapp, B.S. (1993). The anterior cerebellar vermis: essential involvement in classically conditioned bradycardia in the rabbit. J Neurosci *13*, 3705-3711. 10.1523/JNEUROSCI.13-09-03705.1993.
34. Chen, C.H., Williams, J.L., and Lutherer, L.O. (1994). Cerebellar lesions alter autonomic responses to transient isovolaemic changes in arterial pressure in anaesthetized cats. Clin Auton Res *4*, 263-272. 10.1007/BF01827432.
35. Armstrong, D.M., Rotler, A., Hersh, L.B., and Pickel, V.M. (1988). Localization of choline acetyltransferase in perikarya and dendrites within the nuclei of the solitary tracts. J Neurosci Res *20*, 279-290. 10.1002/jnr.490200302.
36. Zhao, Q., Yu, C.D., Wang, R., Xu, Q.J., Dai Pra, R., Zhang, L., and Chang, R.B. (2022). A multidimensional coding architecture of the vagal interoceptive system. Nature *603*, 878-884. 10.1038/s41586-022-04515-5.
37. Caravaca, A.S., Gallina, A.L., Tarnawski, L., Tracey, K.J., Pavlov, V.A., Levine, Y.A., and Olofsson, P.S. (2019). An Effective Method for Acute Vagus Nerve Stimulation in Experimental Inflammation. Front Neurosci *13*, 877. 10.3389/fnins.2019.00877.
38. Altidor, L.K., Bruner, M.M., Deslauriers, J.F., Garman, T.S., Ramirez, S., Dirr, E.W., Olczak, K.P., Maurer, A.P., Lamb, D.G., Otto, K.J., et al. (2021). Acute vagus nerve stimulation enhances reversal learning in rats. Neurobiol Learn Mem *184*, 107498. 10.1016/j.nlm.2021.107498.
39. Kawada, T., Sonobe, T., Nishikawa, T., Hayama, Y., Li, M., Zheng, C., Uemura, K., Akiyama, T., Pearson, J.T., and Sugimachi, M. (2020). Contribution of afferent pathway to vagal nerve stimulation-induced myocardial interstitial acetylcholine release in rats. Am J Physiol Regul Integr Comp Physiol *319*, R517-R525. 10.1152/ajpregu.00080.2020.

40. Vuckovic, A., Tosato, M., and Struijk, J.J. (2008). A comparative study of three techniques for diameter selective fiber activation in the vagal nerve: anodal block, depolarizing prepulses and slowly rising pulses. J Neural Eng *5*, 275-286. 10.1088/1741-2560/5/3/002.
41. Brindley, G.S., and Craggs, M.D. (1980). A technique for anodally blocking large nerve fibres through chronically implanted electrodes. J Neurol Neurosurg Psychiatry *43*, 1083-1090. 10.1136/jnnp.43.12.1083.
42. Ahmed, U., Chang, Y.C., Cracchiolo, M., Lopez, M.F., Tomaio, J.N., Datta-Chaudhuri, T., Zanos, T.P., Rieth, L., Al-Abed, Y., and Zanos, S. (2020). Anodal block permits directional vagus nerve stimulation. Sci Rep *10*, 9221. 10.1038/s41598-020-66332-y.
43. Lu, K.H., Cao, J., Phillips, R., Powley, T.L., and Liu, Z. (2020). Acute effects of vagus nerve stimulation parameters on gastric motility assessed with magnetic resonance imaging. Neurogastroenterol Motil *32*, e13853. 10.1111/nmo.13853.
44. Cunningham, J.T., Mifflin, S.W., Gould, G.G., and Frazer, A. (2008). Induction of c-Fos and DeltaFosB immunoreactivity in rat brain by Vagal nerve stimulation. Neuropsychopharmacology *33*, 1884-1895. 10.1038/sj.npp.1301570.
45. Yap, J.Y.Y., Keatch, C., Lambert, E., Woods, W., Stoddart, P.R., and Kameneva, T. (2020). Critical Review of Transcutaneous Vagus Nerve Stimulation: Challenges for Translation to Clinical Practice. Front Neurosci *14*, 284. 10.3389/fnins.2020.00284.
46. Yuan, H., and Silberstein, S.D. (2016). Vagus Nerve and Vagus Nerve Stimulation, a Comprehensive Review: Part II. Headache *56*, 259-266. 10.1111/head.12650.
47. Cao, J., Lu, K.H., Powley, T.L., and Liu, Z. (2017). Vagal nerve stimulation triggers widespread responses and alters large-scale functional connectivity in the rat brain. PLoS One *12*, e0189518. 10.1371/journal.pone.0189518.
48. Pnevmatikakis, E.A., Soudry, D., Gao, Y., Machado, T.A., Merel, J., Pfau, D., Reardon, T., Mu, Y., Lacefield, C., Yang, W., et al. (2016). Simultaneous Denoising, Deconvolution, and Demixing of Calcium Imaging Data. Neuron *89*, 285-299. 10.1016/j.neuron.2015.11.037.

49. Agetsuma, M., Sato, I., Tanaka, Y.R., Carrillo-Reid, L., Kasai, A., Noritake, A., Arai, Y., Yoshitomo, M., Inagaki, T., Yukawa, H., et al. (2023). Activity-dependent organization of prefrontal hub-networks for associative learning and signal transformation. Nat Commun *14*, 5996. 10.1038/s41467-023-41547-5.
50. Moran, T.H., and Kinzig, K.P. (2004). Gastrointestinal satiety signals II. Cholecystokinin. Am J Physiol Gastrointest Liver Physiol *286*, G183-188. 10.1152/ajpgi.00434.2003.
51. Rogers, R.C., and Hermann, G.E. (2008). Mechanisms of action of CCK to activate central vagal afferent terminals. Peptides *29*, 1716-1725. 10.1016/j.peptides.2008.06.023.
52. Yamada, D., Koppensteiner, P., Odagiri, S., Eguchi, M., Yamaguchi, S., Yamada, T., Katagiri, H., Wada, K., and Sekiguchi, M. (2017). Common Hepatic Branch of Vagus Nerve-Dependent Expression of Immediate Early Genes in the Mouse Brain by Intraportal L-Arginine: Comparison with Cholecystokinin-8. Front Neurosci *11*, 366. 10.3389/fnins.2017.00366.
53. Cox, J.E., and Randich, A. (1997). CCK-8 activates hepatic vagal C-fiber afferents. Brain Res *776*, 189-194. 10.1016/s0006-8993(97)01036-6.
54. Altschuler, S.M., Bao, X.M., Bieger, D., Hopkins, D.A., and Miselis, R.R. (1989). Viscerotopic representation of the upper alimentary tract in the rat: sensory ganglia and nuclei of the solitary and spinal trigeminal tracts. J Comp Neurol *283*, 248-268. 10.1002/cne.902830207.
55. Bailey, T.W., Appleyard, S.M., Jin, Y.H., and Andresen, M.C. (2008). Organization and properties of GABAergic neurons in solitary tract nucleus (NTS). J Neurophysiol *99*, 1712-1722. 10.1152/jn.00038.2008.
56. Cooper, C.M., Farrand, A.Q., Andresen, M.C., and Beaumont, E. (2021). Vagus nerve stimulation activates nucleus of solitary tract neurons via supramedullary pathways. J Physiol *599*, 5261-5279. 10.1113/JP282064.
57. Blackshaw, L.A., and Grundy, D. (1990). Effects of cholecystokinin (CCK-8) on two classes of gastroduodenal vagal afferent fibre. J Auton Nerv Syst *31*, 191-201. 10.1016/0165-1838(90)90185-l.
58. Lock, M., Alvira, M., Vandenberghe, L.H., Samanta, A., Toelen, J., Debyser, Z., and Wilson, J.M. (2010). Rapid, simple, and versatile manufacturing of

936 recombinant adeno-associated viral vectors at scale. Hum Gene Ther *21*, 1259-
937 1271. 10.1089/hum.2010.055.
938 59. Shibata, A.C.E., Ueda, H.H., Eto, K., Onda, M., Sato, A., Ohba, T., Nabekura, J.,
939 and Murakoshi, H. (2021). Photoactivatable CaMKII induces synaptic plasticity
940 in single synapses. Nat Commun *12*, 751. 10.1038/s41467-021-21025-6.
941 60. Agetsuma, M., Hamm, J.P., Tao, K., Fujisawa, S., and Yuste, R. (2018).
942 Parvalbumin-Positive Interneurons Regulate Neuronal Ensembles in Visual
943 Cortex. Cereb Cortex *28*, 1831-1845. 10.1093/cercor/bhx169.
944 61. Davis, S.F., Derbenev, A.V., Williams, K.W., Glatzer, N.R., and Smith, B.N.
945 (2004). Excitatory and inhibitory local circuit input to the rat dorsal motor
946 nucleus of the vagus originating from the nucleus tractus solitarius. Brain Res
947 *1017*, 208-217. 10.1016/j.brainres.2004.05.049.
948 62. Evangelidis, G.D., and Psarakis, E.Z. (2008). Parametric image alignment using
949 enhanced correlation coefficient maximization. IEEE Trans Pattern Anal Mach
950 Intell *30*, 1858-1865. 10.1109/TPAMI.2008.113.

951

952 **Figures (from next page)**

953

Figure. 1

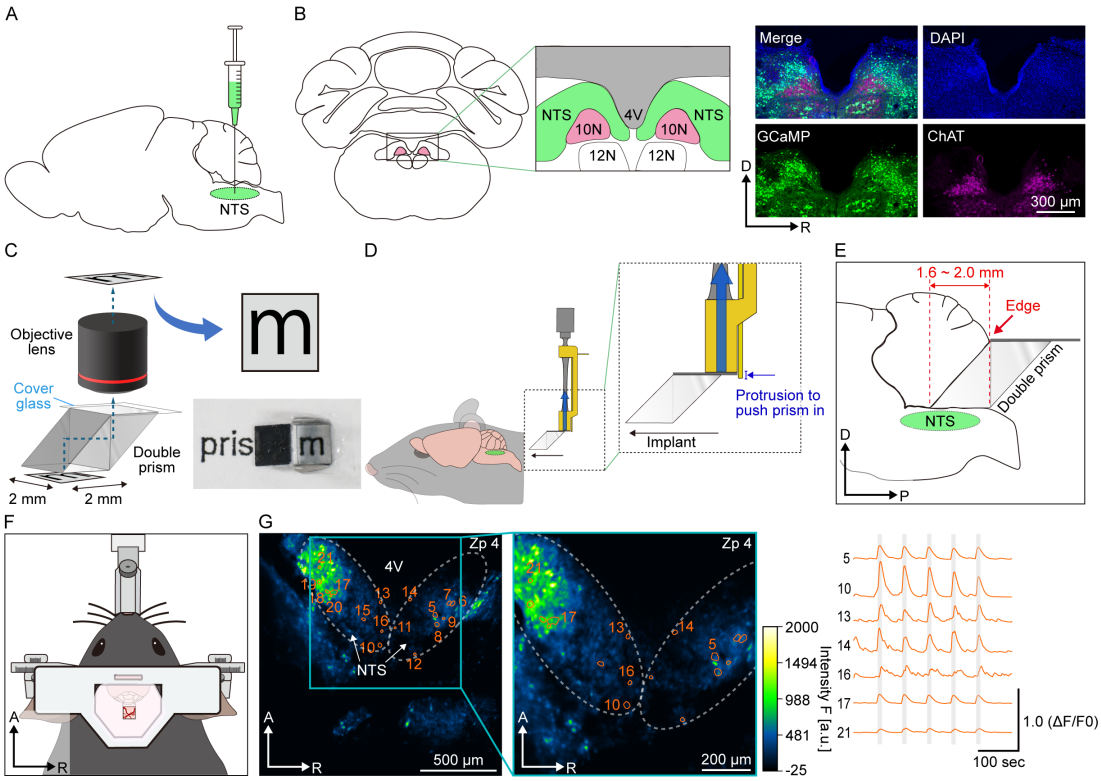

Figure 1. Schematic overview of *in vivo* NTS imaging with a double prism

(A) Sagittal view of a mouse brain illustrating how GCaMP was expressed in NTS neurons by AAV injection.

(B) GCaMP expression in the NTS (coronal view). (left) Schematic illustration of the injection site modified from the Allen Brain Atlas. (right) Expression of GCaMP (green) in the NTS, exclusive to the 10N area (marked by ChAT immunohistochemical staining in magenta). Blue, DAPI.

(C) Two 2-mm right-angled prisms are attached to each other using UV-curable optical adhesive and bonded to a 3 mm × 3 mm square cover glass. In this illustration, the letter "m" at the bottom of the double prism appears through the double prism and the objective lens. Similarly, in the picture at the right bottom corner, the letter "m" in the word "prism" appears through the double prism.

(D) A vacuum-type prism holder is used to implant the double prism. Black arrows indicate the directions in which the double prisms are pushed forward. Thick blue arrows indicate directions in which the double prisms are vacuumed up to be held by the holder. A thin blue

arrow indicates the protrusion to push the double prism during the implantation.

(E) Implantation of the double prism. The double prism is carefully inserted between the cerebellum and the brainstem approximately 1.6−2.0 mm from the posterior edge of the cerebellum. The area containing the NTS is observed through the double prism.

(F) A head plate is attached to the mouse skull using dental cement after the microprism implantation.

(G) Example of *in vivo* brainstem imaging showing neural activity in a live mouse. Left: Representative two-photon images showing GCaMP fluorescence in a large field of view covering the wide brainstem. Each number in the image indicates a region of interest (ROI), each corresponding to a putative single neuron. Median fluorescence over time is presented in green-fire-blue to show a baseline fluorescence level. Middle: Magnified view of a section from the left panel. Right: Representative traces showing changes in GCaMP signal over baseline ($\Delta F/F0$) in selected ROIs. Gray indicates the timing of VNS. Zp4, 4th z-stacked plane obtained by the volumetric scanning (see also Figure 2A and Figure S3).

D, dorsal; R, right; P, posterior; A, anterior.

Figure. 2

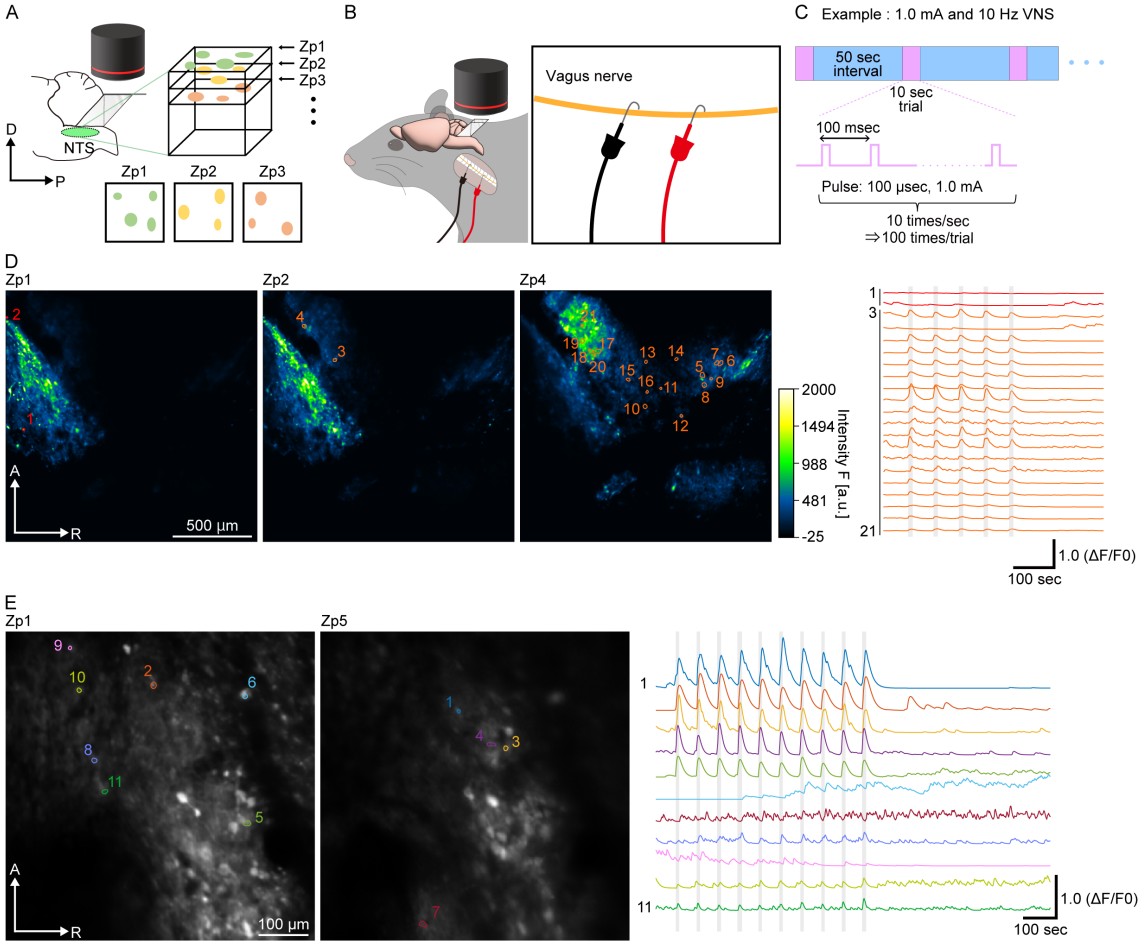

Figure 2. *In vivo* volumetric imaging of NTS activity during repeated VNS

(A) Volumetric live imaging of neural activities in the wide brainstem area, including the NTS. Two-photon imaging was performed through the objective lens (black) and the implanted double prism in the head-fixed mouse under anesthesia. The wide field of view and piezo-based z-scanning enabled volumetric imaging of the GCaMP fluorescence. Colored circles illustrate examples of detected regions of interest (ROIs) at Zp1, Zp2, and Zp3.

(B) *In vivo* NTS imaging was conducted during electrical stimulation of the vagus nerve through a bipolar platinum electrode, which wrapped the cervical vagal trunk in a mouse. The electrode was implanted and fixed with the insulating silicone adhesive. To create anodal block for efferent direction, cathode (black) and anode (red) were located on rostral and caudal site of vagus nerve, respectively.

(C) Schematic of VNS protocol. In this example, a 1.0 mA, 10 Hz, 100 μsec train of electrical stimulation was delivered to the left vagus nerve via an electrode. The term "trial" refers to a

1001 VNS with a pulse width of 100 μsec for 10 sec, regardless of frequency and current intensity.
1002 The term "session" is defined as a series of 10-sec VNS presentations at a fixed frequency
1003 and current intensity, with a 50-sec interval, and this example represents a session at 1.0 mA
1004 and 10 Hz.
1005 (D) An example of *in vivo* volumetric imaging of the NTS during VNS at 2.0 mA and 10 Hz.
1006 AAVdj/Syn.GCaMP7f was used for this experiment. (Left) As examples, Zp1, 2, and 4,
1007 which contain automatically detected ROIs in this mouse, are shown (Zp4 here is the same
1008 data as Figure 1G). Median fluorescence over time for each panel is presented in green-fire-
1009 blue to show a baseline fluorescence level. (Right) Detection of spontaneous and/or VNS-
1010 evoked neural activities (ΔF/F0) from 21 example neurons outside (red) and inside (orange)
1011 the NTS. See also Supplementary Movie1.
1012 (E) Higher-magnification imaging provides clear single-cellular precision. NTS imaging was
1013 performed during VNS at 0.5 mA and 10 Hz. AAV1/Syn.GCaMP6f was used for this
1014 experiment. (Left) As examples, Zp1, and 5, which contain automatically detected ROIs in
1015 this mouse, are shown. To clearly distinguish the ROIs by color, median GCaMP fluorescence
1016 in the NTS is shown in grayscale. (Right) Eleven ROIs, each corresponding to a putative
1017 single neuron, are sorted by the magnitude of their responses to the VNS. See also
1018 Supplementary Movie2.
1019 Zp, z-stacked horizontal plane obtained by the volumetric scanning. Gray indicates the timing of
1020 VNS. D, dorsal; P, posterior; A, anterior; R, right.

Figure. 3

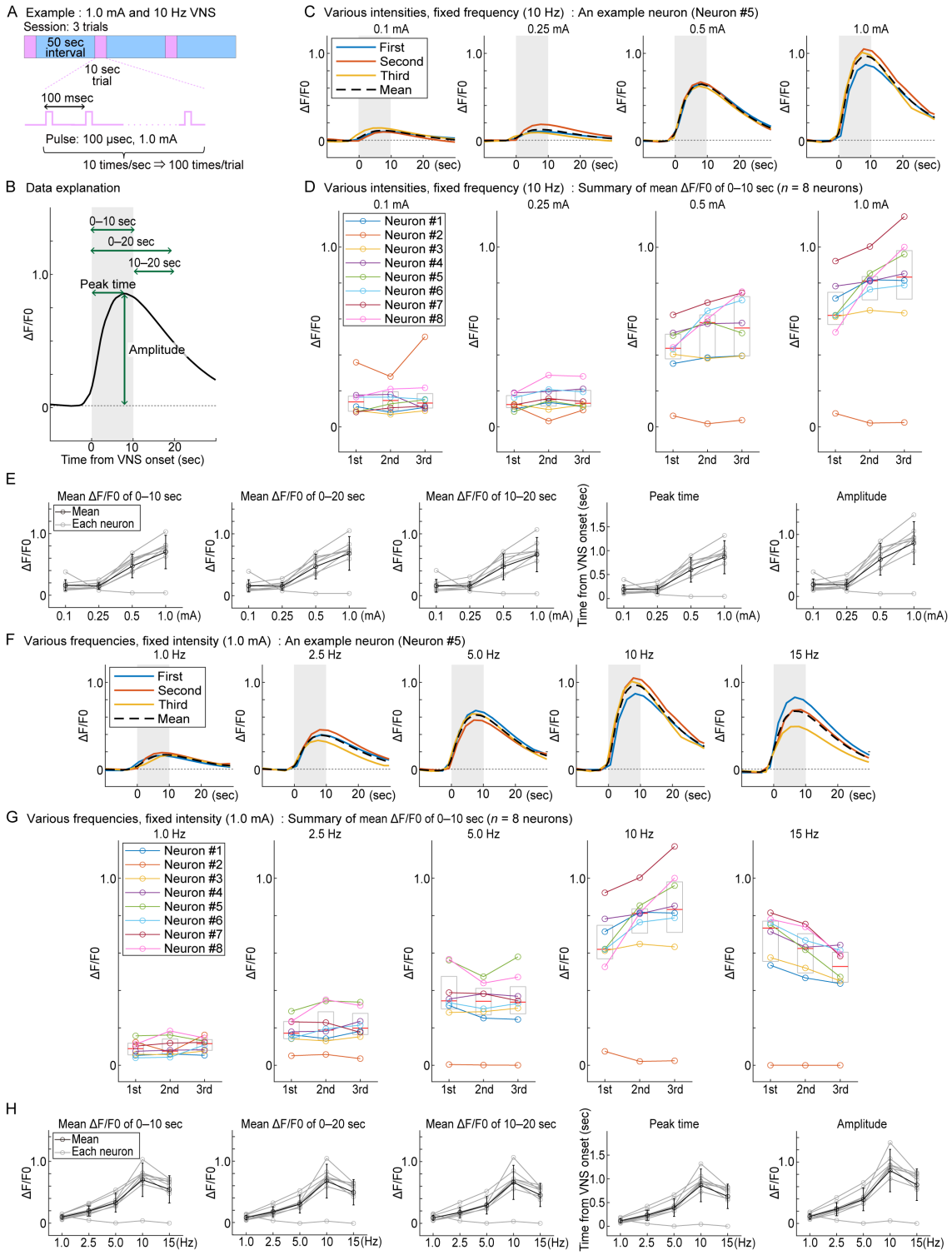

Figure 3. Variable responsiveness of NTS neurons characterized by various VNS conditions (A) Schematic of VNS protocol. In this example, a 1.0 mA, 10 Hz, 100 μsec train of electrical

stimulation was delivered. Each experiment in this figure includes a session consisting of three trials of 10-sec VNS presentations, with a 50-sec interval.

(B) Various parameters for evaluating neural responses. The neural response (ΔF/F0) to VNS (gray shaded area), with the horizontal axis representing the time from the VNS onset. Average signal (0−10, 0−20, 10−20 sec), peak time, and amplitude, which are calculated for evaluating neural responses are indicated by green arrows.

(C) Neural responses of an example neuron to VNS at a fixed frequency of 10 Hz, with various stimulus intensities. Colored lines indicate the neural response to the first, second, and third VNS. Dashed line indicates the mean of the responses to three VNSs.

(D) Summary of responses of simultaneously recorded neurons (n = 8 neurons in a mouse) to VNS at a fixed frequency of 10 Hz with various stimulus intensities. The mean ΔF/F0 of each neuron for 10 sec from the onset of the VNS at various stimulus intensities are summarized.

(E) Summary of neuronal responses to VNS at a fixed frequency of 10 Hz, with various stimulus intensities. Mean values for three trials, for each neuron (gray line) or for all neurons (black line), were calculated. Mean ΔF/F0 of 0–10 sec: the mean of ΔF/F0 for 10 sec from the onset of the VNS. Mean ΔF/F0 of 0−20 sec: the mean of ΔF/F0 for 20 sec from the onset of the VNS. Mean ΔF/F0 of 10–20 sec: the mean of ΔF/F0 for 10 sec from the offset of the VNS. Peak time: time from the VNS onset to the ΔF/F0 peak. Amplitude: ΔF/F0 peak amplitude at each VNS presentation.

(F) An example of ΔF/F0 of neuronal responses to VNS at a fixed stimulus intensity of 1.0 mA, with various frequencies. Colored lines indicate the neural response to the first, second, and third VNS. Dashed line indicates mean of the responses to three VNSs.

(G) Summary of simultaneously recorded neurons (n = 8 neurons in a mouse) to VNS at a fixed stimulus intensity of 1.0 mA, with various frequencies. The mean ΔF/F0 of each neuron for 10 sec from the onset of the VNS at various stimulus frequencies are summarized.

(H) Summary of neuronal responses to VNS at a fixed stimulus intensity of 1.0 mA, with various frequencies. Mean values for three trials, for each neuron (gray line) or for all neurons (black line), were calculated. Mean ΔF/F0 of 0–10 sec, mean ΔF/F0 of 0–20 sec, mean ΔF/F0 of 10–20 sec, peak time, and amplitude were calculated as described in the legend of E.

AAV1/Syn.GCaMP6s was used for this experiment. Gray shaded area indicates the timing of VNS. Boxes in D and G, 25th–75th percentile; Red bars in D and G, median of all neurons. Error bars in E and H, standard deviation.

Figure. 4

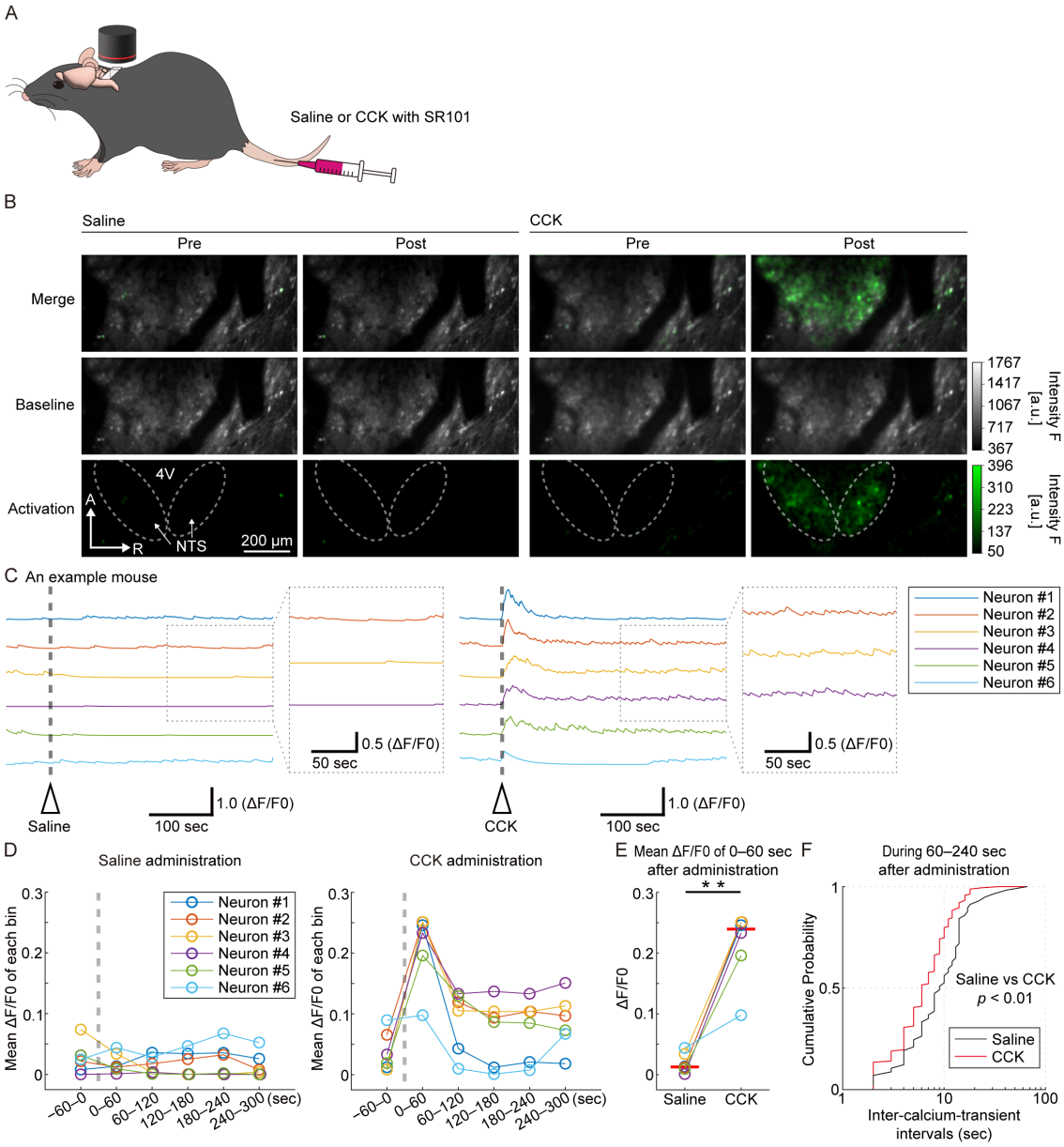

Figure 4. Imaging NTS neural activity in response to intravenous CCK administration

(A) Schematic of *in vivo* NTS imaging while Saline or CCK was administered into the tail vein of an anesthetized mouse (co-administered with red fluorescent dye, SR101). Note that CCK administration was performed more than 10 min after saline administration.

(B) Averaged fluorescence of GCaMP signals during pre- and post-administration (60 sec duration) of Saline or CCK. (Top) Baseline-subtracted signal is shown in green over a background of the baseline image shown in gray, (middle) baseline fluorescence image, (bottom) GCaMP signal. Dashed circles indicates the NTS area. 4V, fourth ventricle. See also

1067 Supplementary Movies 4 and 5.

1068 (C) Traces of GCaMP fluorescence in simultaneously recorded NTS neurons (same neurons on
1069 the left and right). The timings of the injections (saline, left; CCK, right) are indicated by a
1070 gray dotted line. Traces regarding more than five minutes after the injection are expanded to
1071 visualize the higher frequency of spontaneous activity (i.e., frequent calcium transients)
1072 uniquely observed after CCK administration.

1073 (D) The mean ΔF/F0 for each 60-sec bin along the time course was calculated for saline (left) or
1074 CCK (right) administration. Each data point represents the mean ΔF/F for each neuron in each
1075 bin.

1076 (E) The mean ΔF/F for 60 sec immediately after the administration of saline or CCK. Horizontal
1077 red bars, median of all neurons at each condition (saline or CCK). $^{**}p < 0.01$, two-tailed
1078 Wilcoxon signed-rank test ($p = 0.0011$).

1079 (F) The cumulative distribution of intervals between calcium transient events from 60 to 240
1080 seconds after the administration of saline or CCK. Neural activation was evaluated by
1081 detecting the timing of the calcium transients as described in Figure S6 (see also the Methods
1082 for more details). Data from all neurons (6 neurons shown in C) were pooled for each group
1083 for statistical comparison. $^{**}p < 0.01$, Kolmogorov-Smirnov test ($p = 0.0075$).

1084 AAVdj/Syn.GCaMP7f was used for this experiment.

Supplementary Materials

Supplementary Materials (Figures. S1 to S6, and caption for Supplementary Movies S1 to S5) are explained in a separate document.

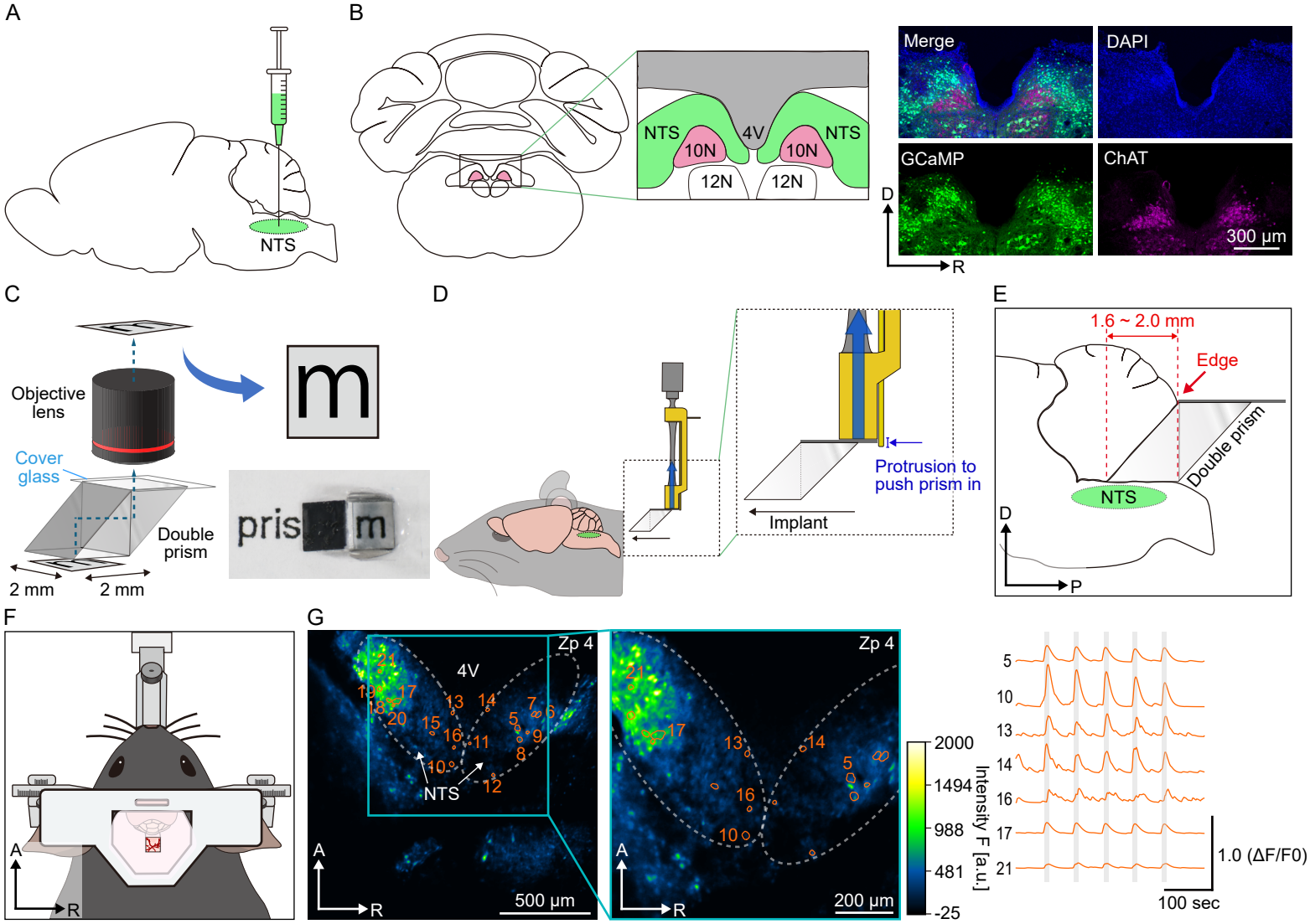
A
NTS
B
NTS
4V
NTS
10N
10N
12N
12N
Merge
DAPI
GCaMP
ChAT
300 μm
D
R
C
Objective lens
Cover glass
Double prism
2 mm
2 mm
m
pris
m
D
Protrusion to push prism in
Implant
E
1.6 ~ 2.0 mm
Edge
Double prism
NTS
D
P
F
A
R
G
Zp 4
4V
NTS
500 μm
Zp 4
200 μm
2000
1494
988
481
-25
Intensity F [a.u.]
5
10
13
14
16
17
21
1.0 (ΔF/F0)
100 sec

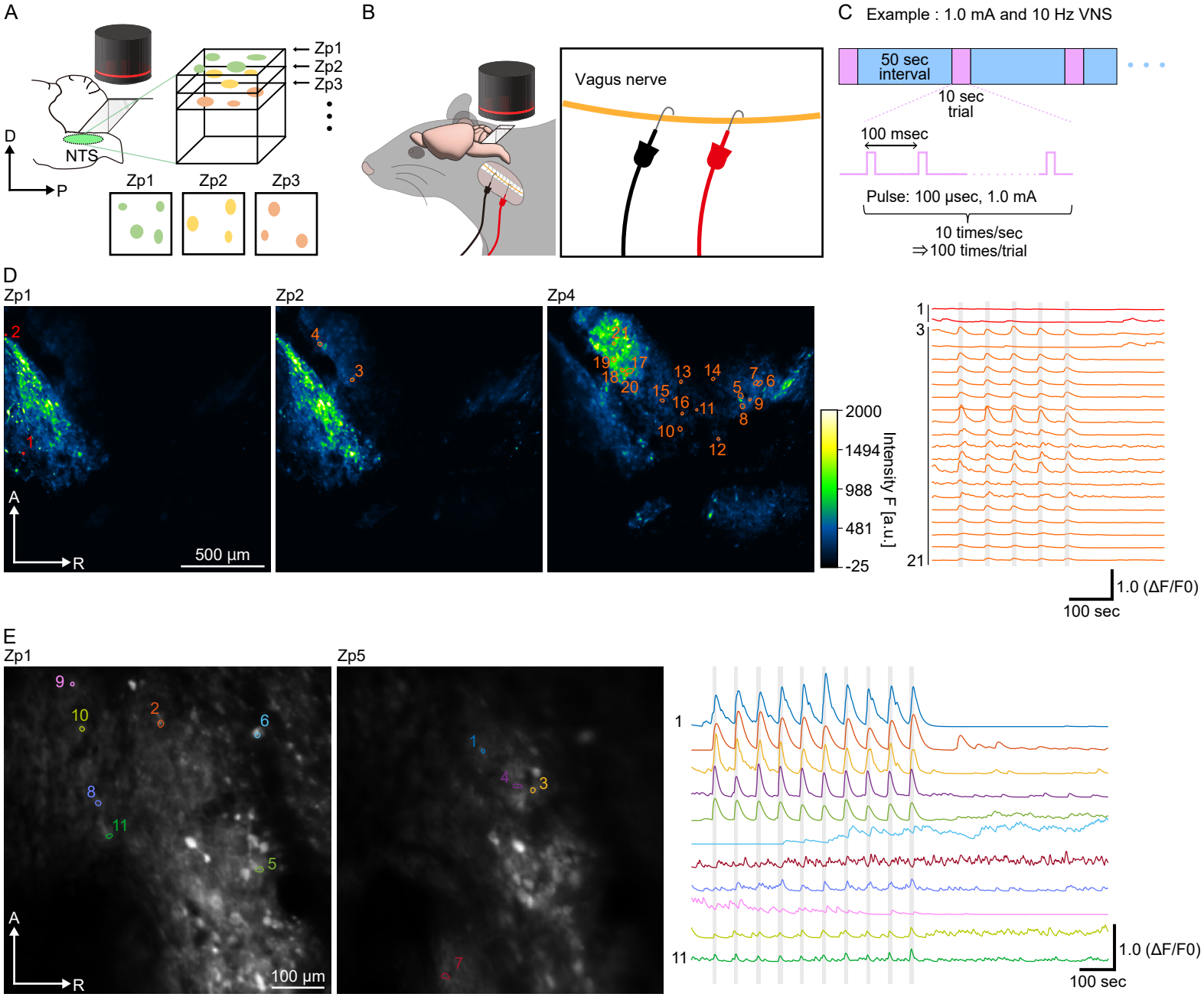
A
Zp1
Zp2
Zp3
D
P
NTS
B
Vagus nerve
C
Example : 1.0 mA and 10 Hz VNS
50 sec interval
10 sec trial
100 msec
Pulse: 100 μsec, 1.0 mA
10 times/sec
⇒100 times/trial
D
Zp1
Zp2
Zp4
A
R
500 μm
2000
1494
988
481
-25
Intensity F [a.u.]
1.0 (ΔF/F0)
100 sec
E
Zp1
Zp5
100 μm
1.0 (ΔF/F0)
100 sec

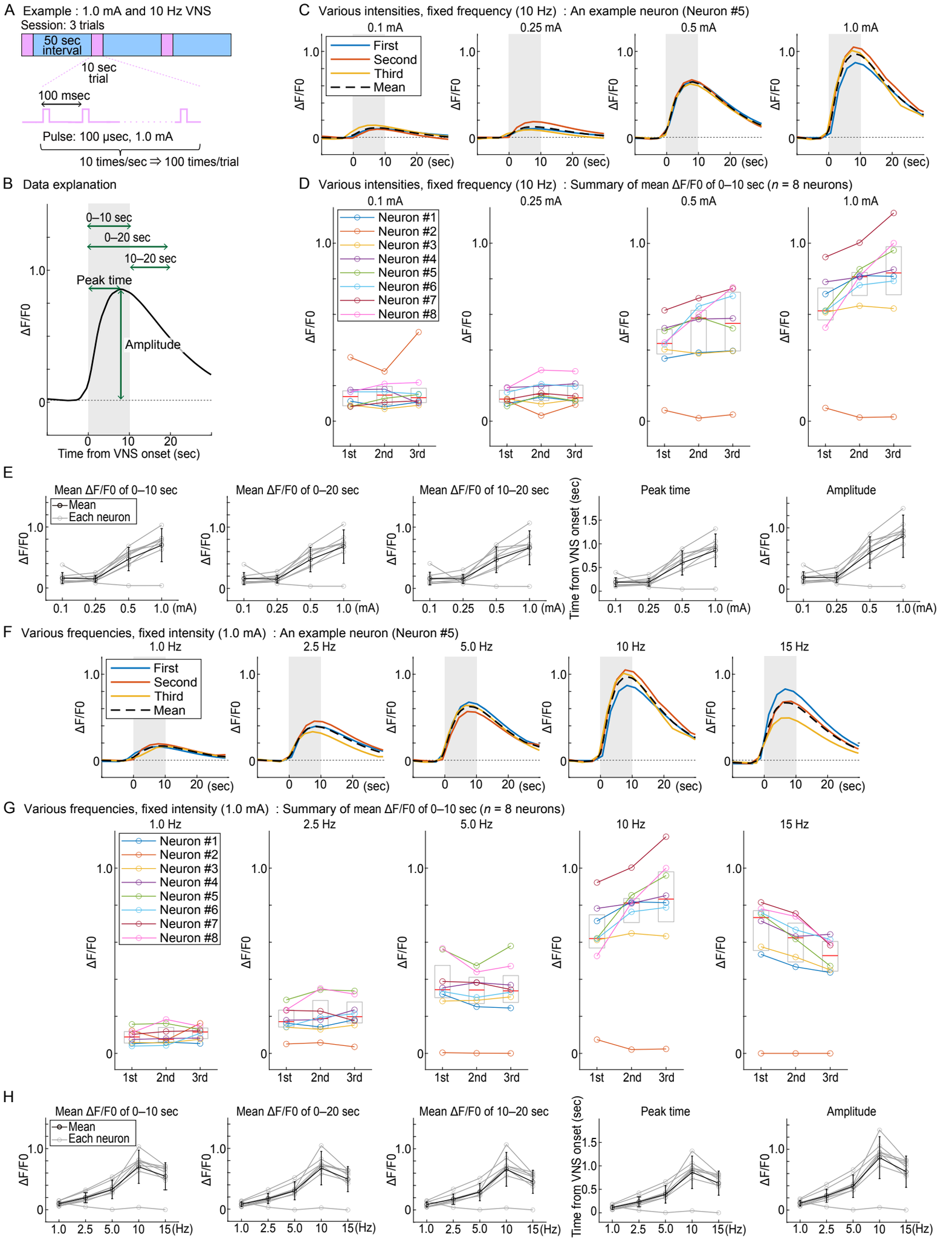
A Example : 1.0 mA and 10 Hz VNS
Session: 3 trials
50 sec interval
10 sec trial
100 msec
Pulse: 100 μsec, 1.0 mA
10 times/sec ⇒ 100 times/trial
B Data explanation
0–10 sec
0–20 sec
10–20 sec
Peak time
Amplitude
ΔF/F0
Time from VNS onset (sec)
C Various intensities, fixed frequency (10 Hz) : An example neuron (Neuron #5)
0.1 mA
0.25 mA
0.5 mA
1.0 mA
First
Second
Third
Mean
ΔF/F0
(sec)
D Various intensities, fixed frequency (10 Hz) : Summary of mean ΔF/F0 of 0–10 sec (n = 8 neurons)
Neuron #1
Neuron #2
Neuron #3
Neuron #4
Neuron #5
Neuron #6
Neuron #7
Neuron #8
1st
2nd
3rd
E
Mean ΔF/F0 of 0–10 sec
Mean ΔF/F0 of 0–20 sec
Mean ΔF/F0 of 10–20 sec
Peak time
Amplitude
Mean
Each neuron
Time from VNS onset (sec)
(mA)
F Various frequencies, fixed intensity (1.0 mA) : An example neuron (Neuron #5)
1.0 Hz
2.5 Hz
5.0 Hz
10 Hz
15 Hz
G Various frequencies, fixed intensity (1.0 mA) : Summary of mean ΔF/F0 of 0–10 sec (n = 8 neurons)
H
(Hz)

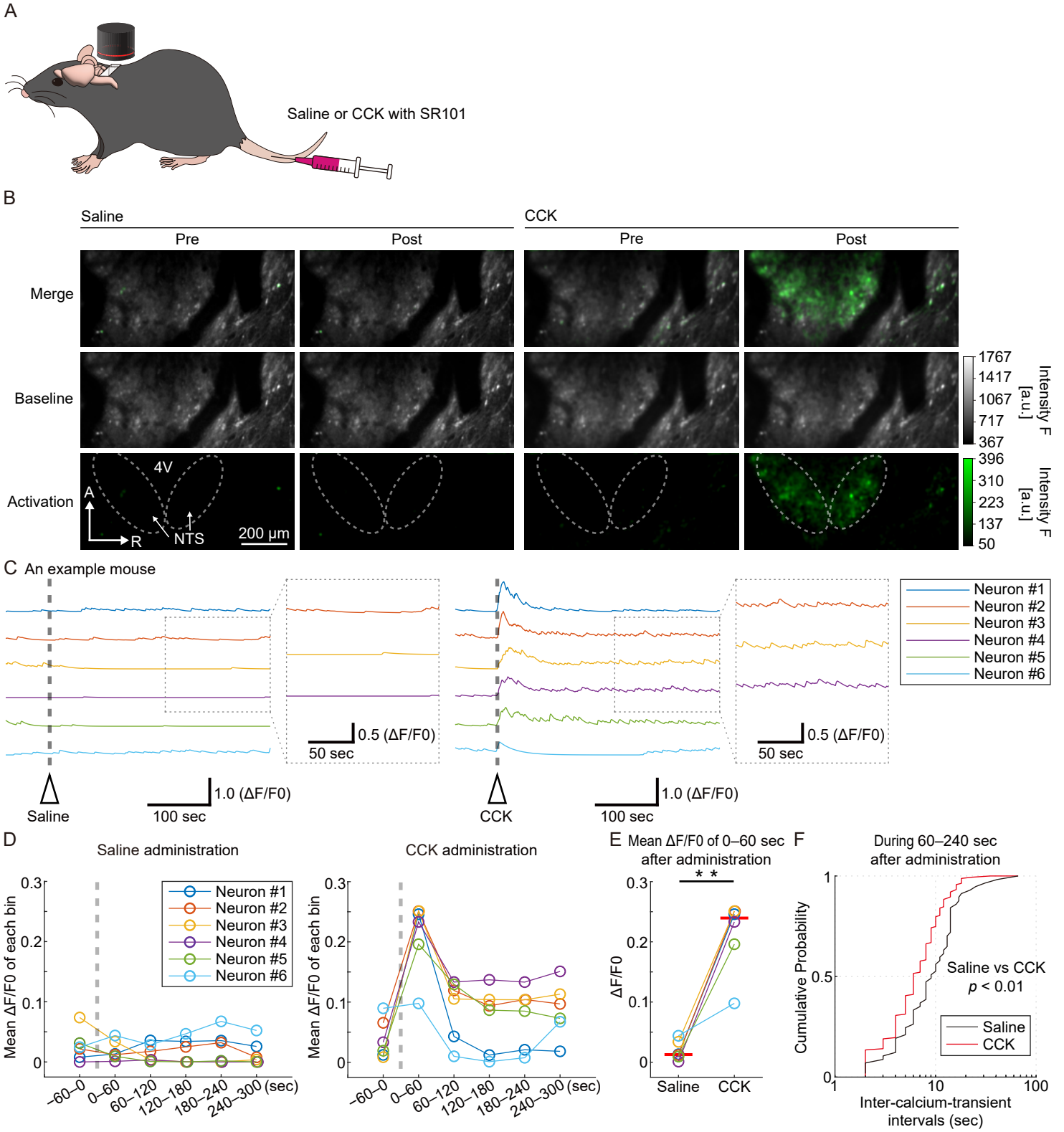
A
Saline or CCK with SR101
B
Saline
CCK
Pre
Post
Pre
Post
Merge
Baseline
Activation
4V
A
R
NTS
200 μm
1767
1417
1067
717
367
Intensity F [a.u.]
396
310
223
137
50
Intensity F [a.u.]
C An example mouse
Neuron #1
Neuron #2
Neuron #3
Neuron #4
Neuron #5
Neuron #6
0.5 (ΔF/F0)
50 sec
1.0 (ΔF/F0)
100 sec
Saline
CCK
D
Saline administration
CCK administration
Mean ΔF/F0 of each bin
0.3
0.2
0.1
0
−60–0
0–60
60–120
120–180
180–240
240–300 (sec)
E Mean ΔF/F0 of 0–60 sec after administration
* *
ΔF/F0
Saline
CCK
F
During 60–240 sec after administration
Cumulative Probability
1
0.5
0
Saline vs CCK
p < 0.01
Saline
CCK
1
10
100
Inter-calcium-transient intervals (sec)